This is a repository copy of *A modified rule-based energy management scheme for optimal operation of a hybrid PV-wind-Stirling engine integrated multi-carrier energy system*.

White Rose Research Online URL for this paper:
https://eprints.whiterose.ac.uk/188878/

Version: Published Version

Article:

eprints@whiterose.ac.uk
https://eprints.whiterose.ac.uk/
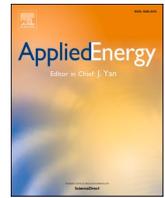
A modified rule-based energy management scheme for optimal operation of a hybrid PV-wind-Stirling engine integrated multi-carrier energy system

Godfrey T. Udeh [a,b,*], Stavros Michailos [a], Derek Ingham [a], Kevin J. Hughes [a], Lin Ma [a], Mohamed Pourkashanian [a]

[a] Energy 2050, Department of Mechanical Engineering, University of Sheffield, Sheffield S3 7RD, United Kingdom
[b] Department of Mechanical Engineering, Faculty of Engineering, University of Port Harcourt, Nigeria

HIGHLIGHTS

- New rule-based schemes have been proposed to manage a multi-carrier energy system.
- Number of system components is obtained by implementing a bi-level optimisation.
- Optimal system's performance in a test location has been examined for a 48 h period.
- Back-up commitment reduces with increasing splits, but its start-up soars by 36%.
- Dumped power and emissions decline with increase in split back-up but cost deepens.

GRAPHICAL ABSTRACT
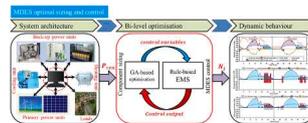
ARTICLE INFO

ABSTRACT

In this study, rule-based energy management strategies (EMS) based on the modifications of the traditional load following (LF) and circuit charging (CC) have been proposed and developed to effectively coordinate the operation of an integrated multi-carrier hybrid energy system. The proposed EMS aim to overcome some of the challenges of the traditional rule-based EMS and broaden their application to the management of complex energy systems. The study deploys a bi-level optimisation scheme to obtain the optimal number of system components that simultaneously minimises the cost, reliability and emissions, in the outer-loop and implements the rule-based EMS in the inner-loop. Also, the results of the optimal system have been simulated for a 48 h timespan, to investigate the effects of the proposed EMS on the Stirling back-up start-ups, battery storage limits, and generation of other energy vectors. The results indicate the deployment of split back-up and batteries minimise the commitment of the back-up, dumped power and emissions. However, the number of start-ups of the back-up increases appreciably by 15.34% and 36%, with the deployment of 2-split and 4-split Stirling, respectively in CC with battery storage. Correspondingly, the operational cost of the system rises as the number of splits increases, but only a slight change in the energy cost is observed, because of the significant reductions in the capacity of the green generators. Interestingly, the batteries record many duty cycles, store less energy and attain lower discharge limits as many small capacity ST back-ups are deployed. Other results demonstrate the additional capabilities of the proposed EMS in handling complex energy systems by the substantial increase in the generation of heating and cooling with increasing splits of the back-up and inclusion of batteries in the optimal system.

Nomenclature

General

c	unit cost $(\frac{\$}{kg}\ or\ \$/l)$
n	component life $(year)$
v	wind speed (m/s)
A	area (m^2)
C	cost $(\$)$, capacity (Ah)
COE	cost of energy, $(\$/kWh)$
F	power loss (W)
G	solar irradiance $\left(\frac{W}{m^2}\right)$
HV	heating value (J/kg)
LCE	life cycle emissions $(kgCO_2)$
N	number $(-)$
P	power (W)
T	temperature (K)
V	voltage (V)
Z	height (m)

Abbreviations

BSS	battery storage system
CC	circuit charging
CHP	combined heat and power
DG	diesel generator
EMS	Energy management system
FC	fuel consumption
HRES	hybrid renewable energy system
GHG	greenhouse gas
ICE	Internal combustion engine
LF	load following
MDES	multi-carrier decentralised energy system
MILP	mixed integer linear programming
MT	Micro turbine
ORC	organic Rankine cycle
PV	photovoltaic
SOC	state of charge
ST	stirling engine

STC	standard test condition
UC	unit commitment
WT	wind turbine

Subscript

a	ambient
ave	average
bat	battery
c	cell
ch	charge
$disch$	discharge
gen	generation
h	horizontal
inf	inflation
int	interest
k	shape factor
l	load
max	maximum
min	minimum
o	surface
p	parallel
r,R	Rate
ref	reference
rep	replacement
s	serial
Ann	annualised
c	scale index
C	cut-in
F	cut-out

Superscript

F	fuel

Greek

α	temperature coefficient $(\%/°C)$
σ	standard deviation $(-)$
$\bar{x}$	mean $(-)$
χ	emission factor $(kgGHG/kgfuel)$

1. Introduction

Multi-carrier decentralised energy systems (MDES) deploy a number of dispatchable and non-dispatchable energy generating and storage units, to satisfy customer energy needs. The effective management of the flow of energy in the numerous generation and storage units that comprise a MDES is crucial to reduce system operational cost, improve efficiency and reliability [1]. Consequently, an energy management system (EMS) is required to efficiently programme the flow of energy through the generating and storage units of a MDES and for its subsequent dispatch to satisfy the loads. EMS are mainly deployed to ensure the continuous supply of energy to the load, maximise the renewable energy penetration, minimise the cost of energy, ensure components protection due to overloading of the system and increase the stability of the energy system [1]. In the literature, heuristic, fuzzy-logic, unit commitment (UC) problem based and smart tools have been proposed as EMS approaches for different energy system configurations [1,2].

Traditionally, the load following scheme (LF), circuit charging (CC) and peak shaving are the popular heuristic energy management schemes deployed in managing the flow of energy in a hybrid renewable energy system (HRES) [2,3]. These dispatch strategies have extensive application in the management of the operation of HRES in the literature. Unfortunately, the traditional heuristic approaches present some challenges. The deployment of the back-up to follow the load in the LF

mode results in the engine operating outside its rated conditions. As a result, the back-up consumes more fuel, which leads to higher emissions and increases the operating cost of the system [4]. On the other hand, the CC mode is characterised by the excessive dumping of power [5,6] and the frequent charging and discharging of the batteries that is inimical to the component's life [7,8]. While the peak shaving presents problem of over sizing of the system leading to excessive dumping of power [9]. There have been attempts to solve these challenges by proposing a hybrid of the LF and CC [10] and the deployment of several small back-ups in CC [11,12]. Das et al. [12] compared the cost of energy (COE), life cycle emissions (LCE) and excess power generated from a solar photovoltaic (PV) system when one large and two small capacities internal combustion engine (ICE) and micro-turbine (MT) were deployed as the back-up, respectively. The recorded COE in both cases were comparable, due to the fewer number of PV panels deployed in the split back-up case, thereby neutralising the high initial cost of the back-ups. However, they observed the system with split back-up emits more harmful gases but reduces excessive dumping of power compared to the one large capacity back-up case.

In more complex energy systems, the EMS is implemented in the form of a unit commitment (UC) scheduling problem, by formulating mixed integer linear (or non-linear) programming (MILP) models [13]. The formulated MILP is solved by deploying the receding horizon approach that relies on the forecasting of the hourly energy demand and

generation from the system units, to schedule its operation [13].

Mazzola et al. [13] proposed a MILP cost minimisation problem to manage the energy of a multi-good system. This study penalises the system for not meeting the demand of any good at a time step and the severity of the penalty is determined by the priority of the good. The scheduling problem is solved over a time horizon based on forecasted weather and demand data for a test location. The MILP approach resulted in savings in the operational cost of the system by 8.5% compared with the CC approach. In Parpergiougio and Silvente [14], a MILP model was formulated to minimise the operational cost of a combined heating and power (CHP) system. The proposed EMS contributes about 5% savings in the system's operational cost and results in significant reductions in power purchases from the grid. Parisio et al. [15] proposed a MILP with a day ahead forecasting of the energy generation and demand to minimise the operating cost of a MDES.

However, most of these studies did not undertake the sizing optimisation of the energy system, which is strongly tied to the energy management of the system. Roshandel and Forough [16] solely determined the optimal number of the components of a hybrid PV, wind turbine (WT), battery storage and diesel generator (DG) back-up system, by minimising the total life cost of the system. Also, the receding horizon has been applied to minimise the real time cost of operation of the optimal system. They observed that with the increment in the length of the prediction horizon, the penetration of the renewable energy resources increases, and this minimises the deployment of the back-up. Although this approach is an improvement over the previous studies, it is still lacking because the EMS of the system is not coupled to its sizing optimisation.

Thus, bi-level optimisation that couples the sizing optimisation and the energy management of the system has been proposed. Li et al. [17] found the optimal configuration and control strategy of a HRES that utilises battery and hydrogen storages, by deploying a bi-level optimisation of the system. The optimal configuration of the HRES was found in the outer-loop by the genetic algorithm (GA), while the EMS was implemented in the inner-loop at every time step of the prediction horizon, based on the minimisation of the MILP model. The proposed approach reportedly reduces the operational cost of the system compared to the rule-based approaches. Similarly, Rullo et al. [18] proposed a bi-level sizing and energy management of a HRES. In this study, the authors jointly considered the economic and reliability functions in determining the optimal size of the components of the HRES in the outer-loop. The inner-loop implements the EMS as a MILP scheduling problem involving cost minimisation.

The UC scheduling EMS approaches offer reduced operational costs when deployed for a day ahead scheduling of the MDES and are more suitable to coordinate co-production of energy vectors and other useful goods. Nonetheless, their reliance on the forecast of the future production of renewable generators and demand of the consumers limit the model accuracy because of the associated prediction errors. In addition, with the increasing complexity of the system, the computational time will increase prolonging the response time in this EMS approach. This is even made worse as the length of the prediction horizon increases [16].

For these reasons, the fuzzy-logic based EMS are becoming very attractive for managing the flow of energy in MDES. They rely on the formulation of some set of rules based on if-then constructs that do not require complex mathematical modelling to manage the system. Several studies have integrated the rule-based EMS with the optimal sizing of the components of a HRES. In these studies, some rules are formulated based on the experience of the designer to manage the system, while key system control variables are optimised by deploying memetic algorithms.

Dufo-lopez et al. [19] proposed a rule-based approach for managing the operation of a hybrid PV, WT, DG and battery storage system. This study optimised the control parameters of the system including the minimum state of charge of the battery, minimum output power and critical power of the DG using the GA. Bukar et al. [20] proposed a fuzzy-logic strategy that deploys four operational modes to coordinate the power generation from a standalone HRES and match it with the energy consumption. Sun et al. [21] initiated a methodology that operates by matching the charging time with the time of use of the energy, to coordinate the charging of electric vehicles with grid power or power generated from a HRES. Lu et al. [22] formulated two rule-based EMS modes to minimise the system operational costs and environmental protective costs of a hybrid WT-PV-DG-MT and vehicle to grid (V2G) system. Bracco et al. [23] developed mathematical models to minimise the daily operational cost of a smart micro-grid that simultaneously supplies electric power, cooling and heating loads to a university campus in Spain and also charge electric vehicles. Bhatti and Salam [24] proposed fuzzy-logic approach to optimise the cost of charging of electric vehicles with power supplied either by a PV-battery system or the grid, with the main goal of achieving a fixed energy price during operation.

Although the rule-based EMS are popular for managing HRES, only a few authors have deployed this approach to manage complex energy systems in which other energy vectors and goods are co-produced. This opportunity needs to be fully explored and it is the main goal of this paper. Further, the deployment of split back-up is promising for reducing the size of the non-programmable generators and minimising the dumped power, which are some of the drawbacks of the traditional heuristic approaches. However, it is not clear how this will impact the performance of the battery storage. Further, as the number of splits of the back-up increases, the frequency of start-ups of the back-up may increase and this could increase the operational cost of the system. Unfortunately, there is limited knowledge of the global impact of the deployment of split back-ups on the cost of energy of the system with or without the inclusion of batteries. Finally, for a multi-carrier energy system, it will be insightful to investigate the impact of the combined inclusion of batteries and split back-up on the generation of other energy vectors.

Therefore, this paper proposes the bi-level integration of the optimal component sizing based on the genetic algorithm and rule-based energy management of a HRES integrated multi-carrier decentralised energy system. Here, some parameters that control the dispatch of the back-up have been optimised in the outer-loop. The obtained optimal system configurations have been dynamically simulated to investigate the impact of the deployment of split Stirling (ST) in the proposed rule-based EMS on the cost, reliability, emissions, dumped power, battery use optimisation and start-up costs of the system.

The main contributions of this paper are:

- Proposing a bi-level approach to determine the optimal configuration of a MDES. The optimal system and control strategy that simultaneously minimises the loss of power supply probability, levelised cost of energy and dumped power is found with a memetic algorithm. Each candidate optimal configuration from the outer-loop is evaluated in the inner-loop based on the proposed rule-based EMS approaches.
- Investigating the global impact of split back-up on the frequency of start-ups of the ST back-up and the associated operational costs as well as the impact on the battery use, by undertaking hourly dynamic simulation of the optimal system. Also, the impact of split ST on the energy cost, reliability, carbon emissions and dumped power will be studied from a broader perspective.
- Examining the overall effects of the proposed rule-based energy management systems on the hourly behaviour of the integrated multi-carrier system, by simulating the system performance for two days of operation. Additional insights into the combined impact of the inclusion of battery storage and split ST on the simultaneous generation of cooling, heating and electricity from the multi-carrier energy system will be gained from the dynamic simulation.

2. Energy system description

Fig. 1 depicts the proposed multi-carrier energy system intended to meet the cooling, heating and electricity demands of the test location: Onye-Okpan community; a coastal community in southern Nigeria (latitude: 5.976515° N and longitude: 8.47067° E) with 500 households. The energy system integrates a HRES that comprises solar PV modules, horizontal axis wind turbines (WT), battery storage, split Stirling engines (ST) and Organic Rankine cycle (ORC) back-up power to an absorption chiller and a waste heat recovery boiler. The ST + ORC back-up plays the dual role of augmenting the reliability of the HRES and driving the heating and cooling system. The flue gas produced from the combustion of woodchips fuel fires the ST, the thermal chiller and the waste heat economiser before being deployed to dry the wet woodchips, while the exhaust waste heat from the ST is recovered to power the ORC.

3. Components modelling and problem formulation

In this section, the modelling of the HRES and back-up components are presented. Further, the optimisation problem is formulated by considering technical, economic and environmental metrics.

3.1. Development of component models

This section presents the mathematical models for predicting the performance of the components of the proposed HRES. These models are the basis for building the objective functions deployed in the sizing optimisation.

3.1.1. Photovoltaic modules

The hourly simulation of the generation of power from the photo-

voltaic models can be obtained from [25]:

$$P_{PV}(t) = P_{STC}\left[\frac{G_h(t)}{G_{STC}}\left(1 + \frac{\alpha}{100}(T_c(t) - T_a(t))\right)\right]F_{diss} \quad (1)$$

where $P_{STC}(W)$ is the module maximum power at standard test conditions, $G_h\left(\frac{W}{m^2}\right)$ is the hourly global solar radiation, $G_{STC}\left(\frac{W}{m^2}\right)$ is the solar radiation at the test conditions, $\alpha(\%/°C)$ is the temperature coefficient, $T_a(°C)$ is the ambient temperature and $F_{diss}(-)$ is a factor that accounts for power dissipation due to dirt, wires, modules mismatch, and other losses.

The cell temperature $T_c(°C)$ is obtained from the following expression [25]:

$$T_c(t) = T_a(t) + \left(\frac{NOCT - 20}{0.8}\right)\frac{G_h(t)}{G_{STC}} \quad (2)$$

where $NOCT(°C)$ is the nominal operating cell temperature.

Consequently, the power produced from the PV array at any time step, t, can be obtained as follows:

$$P_{array}(t) = IV = P_{PV}(t)N_s N_p \quad (3)$$

$N_p(-)$ is the number of PV panels in parallel.

The number of PV modules arranged in series, N_s is given as a function of the bus voltage, V_{bus} and the rated voltage of the PV panel provided by the manufacturer, V_{PV}:

$$N_s = \frac{V_{bus}}{V_{PV}} \quad (4)$$

3.1.2. Wind turbines

The modelling of the power from the wind turbine is presented in this
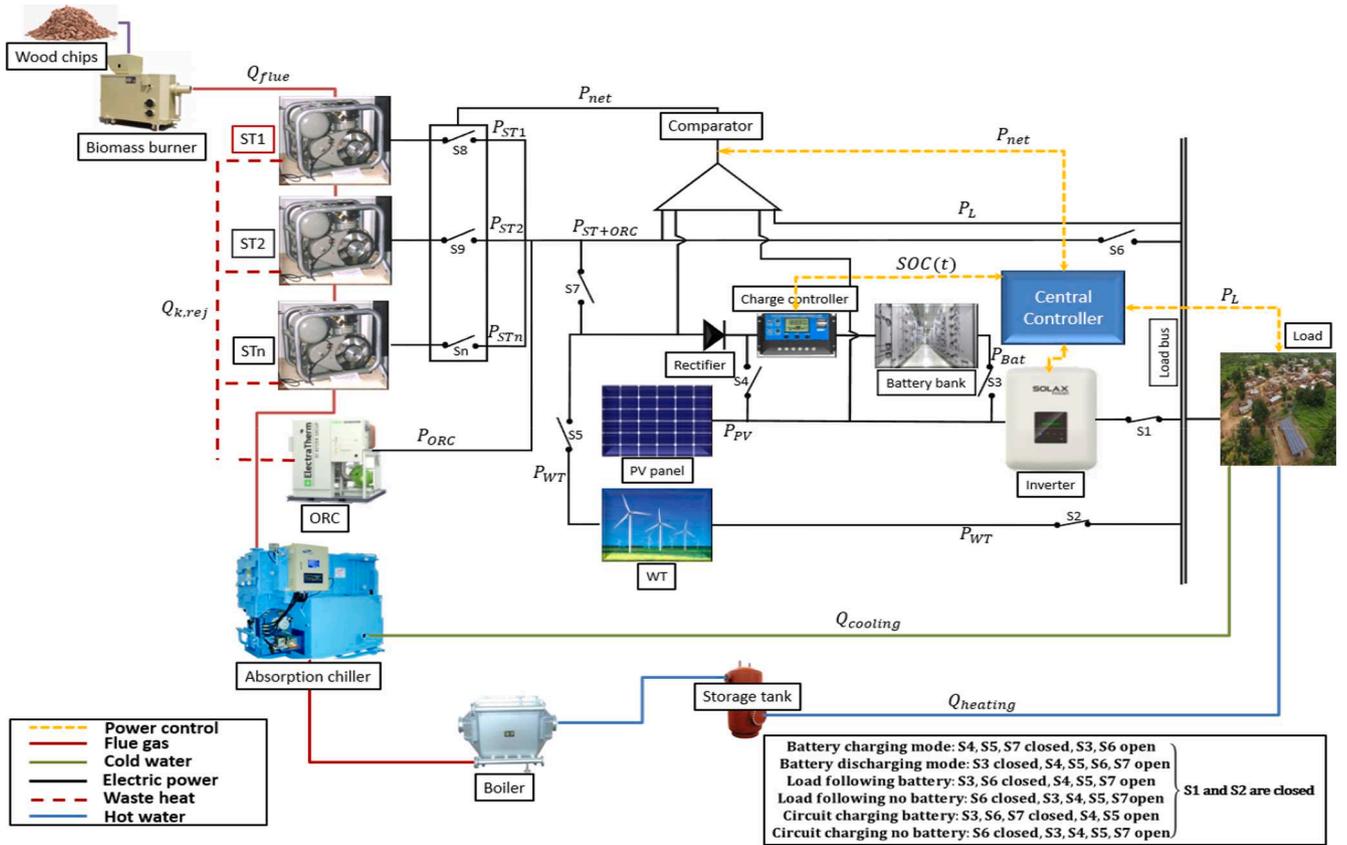
Fig. 1. Schematic of the multi-carrier energy system showing the central controller.

section. The actual power output from the wind turbine can be estimated from the power curve in Fig. 2 which is usually furnished by the manufacturer.

Based on the power curve provided by the manufacturer, the power that can be extracted from a moving stream of air at any given speed and hub height can be quantified directly using the following expression [27–29]:

$$P_{WT}(t) = \begin{cases} \dfrac{\nu^k - \nu_c^k}{\nu_R^k - \nu_c^k}.P_R & \nu_C \leq \nu \leq \nu_R \\ P_R & \nu_R \leq \nu \leq \nu_F \\ 0 & \nu \leq \nu_C \ and \ \nu \geq \nu_F \end{cases} \tag{5}$$

where $\nu(m/s)$ is the wind speed in the test location, $\nu_C(m/s)$ is the cut-in wind speed, $\nu_R(m/s)$ is the rated wind speed, $\nu_F(m/s)$ is the cut-out wind speed and $P_R(W)$ is the rated power of the turbine. The wind speed data at the location has been obtained from PVGIS [30] for a period of one year and was measured at 10 m hub height.

To obtain the wind speed at the hub height of the selected turbines, the following logarithmic law is employed [27,29]:

$$\nu_{hub} = \nu_r.\frac{\ln \frac{Z_{hub}}{Z_0}}{\ln \frac{Z_r}{Z_0}} \tag{6}$$

where ν_{hub} (m/s) is the wind speed at the hub height, Z_{hub} (m) is the desired hub height, $Z_r(m)$ is the reference height, $\nu_r(m/s)$ is the wind velocity at the hub height, $Z_0(m)$ is the surface roughness height.

3.1.3. Combined Stirling and ORC engine

As previously stated, this work proposes a combined ST and ORC as the back-up to the HRES system, deployed to augment the electricity generation from the renewable generators. The power supplied by the combined ST + ORC back-up at any time step is determined by the availability of the renewable generators, the control strategy and the state of charge of the battery. In this study, the biomass fuel consumption of the ST + ORC , FC_{ST+ORC} (kg) will be determined from the energy balance of the heat engine and is expressed as:

$$FC_{ST+ORC}(t) = \frac{3600 P_{gen,ST+ORC}(t)}{\eta_{combustor} HV_{woodchips} \eta_{ST+ORC}} \tag{7}$$

where $P_{gen,ST+ORC}(W)$ is the power delivered by the back-up at a given time step, $\eta_{combustor}(-)$ is the efficiency of the biomass combustor, $HV_{woodchips}$ (J/kg) is the calorific value of woodchips and η_{ST+ORC} $(-)$ is the electrical efficiency of ST + ORC back-up. The combined efficiency of the ST + ORC and combustor efficiency in Eq. (7) have been extracted from Ref. [31,32] and are given as 38 % and 88 %, respectively.

In addition, the greenhouse gas (GHG) emitted by the back-up from each of the proposed control strategies has been modelled, to evaluate the impact of the control strategies on the GHG emissions. The GHG emitted by the ST + ORC is determined according to the guidelines of the international panel on climate change (IPCC) and is given as [33]:

$$y_{GHG}^F = HV_F \chi_{GHG}^F \sum FC_{ST+ORC}(t) \tag{8}$$

where $HV_F(J/kg)$ is the heating value of the fuel, χ_{GHG}^F (g GHG/J fuel) is the emission factor. The value of these constants have been extracted from [33,34] and presented in Table 1.

3.1.4. Battery storage

The battery is one of the dispatchable units deployed to meet the power deficit in the proposed HRES configuration. In this study, the amount of energy the battery supplies or retains is determined by the WT + PV generation, consumer electric load, power dispatching strategy, the state of charge (SOC) of the battery and the power generation from the back-up. At any time, t, the energy stored or released by the

Table 1
Constants for the evaluation of the GHG emissions [33,34].

Woodchips	Value
Heating value (MJ/kg)	19.2
CO_2 Emissions factor (kg Co_2/ MJ)	0.112
N_2O Emissions factor (kg N_2O / MJ)	4.0×10^{-6}
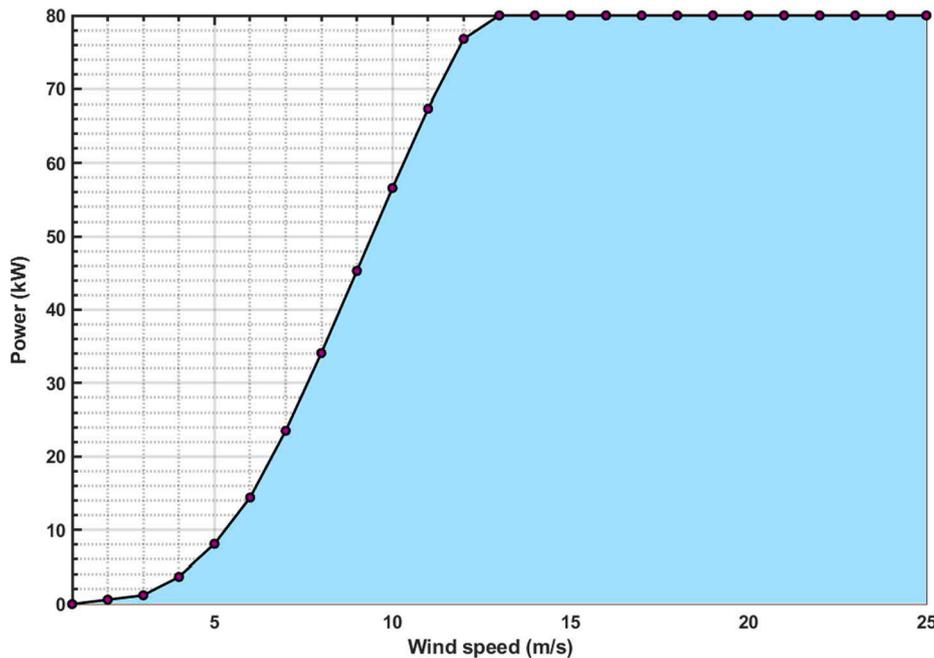
Fig. 2. Power curve of the Enercon E-18 wind turbine [26].

battery banks can be obtained from the following expressions:

Charging :

$$SOC(t+\Delta t) = \begin{cases} SOC(t) + \eta_{ch}\left(\dfrac{(P_{PV}(t) + P_{WT}(t) - P_L(t))}{V_{Bat}}\right)\Delta t/C_{Bat}, LF \\[2em] SOC(t) + \eta_{ch}\left(\dfrac{(P_{PV}(t) + P_{WT}(t) + P_{ST+ORC}(t) - P_L(t))}{V_{Bat}}\right)\Delta t/C_{Bat}, CC \end{cases} \qquad (9)$$

discharging :

$$SOC(t+\Delta t) = SOC(t) - \left(\frac{(P_L(t) - P_{PV}(t) - P_{WT}(t) - P_{ST+ORC}(t))}{\eta_{disch}.V_{Bat}}\right).\Delta t/C_{Bat} \qquad (10)$$

where $\eta_{\mathrm{ch}}(-)$, $\eta_{\mathrm{disch}}(-)$, $V_{\mathrm{Bat}}(\mathrm{V})$, $C_{\mathrm{Bat}}(\mathrm{Ah})$ are the charging efficiency, discharge efficiency, voltage and nominal capacity of the battery, respectively, P_{PV} (W), $P_{\mathrm{WT}}(\mathrm{W})$, and $P_{\mathrm{ST+ORC}}(\mathrm{W})$ are the electric power produced by the PV, WT and ST + ORC, respectively, $P_{\mathrm{L}}(\mathrm{W})$ is the electric load, $\Delta t(\mathrm{s})$ is the time interval. The time interval used in this study is 1 h. The specification and cost of the components of the system are given in Table 2.

4. Formulation of the proposed dispatch strategies

The energy management of an integrated multi-carrier energy system is a critical aspect of the design and operation of the system [18]. Therefore, it is important to consider the EMS at the point of the design

Table 2
Specification of the components of the HRES.

Component	Type	Specification	Value
Batteries (3 types) [35]	Hoppecke Sun AGM	Voltage, (V)	2
		Capacity, (Ah)	1120
	Hoppecke Sun AGM	Voltage, (V)	2
		Capacity, (Ah)	890
	Hoppecke Sun AGM	Voltage, (V)	2
		Capacity, (Ah)	620
Wind turbines (2 types) [26]	EWT DW 52–250 HH40	Cut-in speed, (m/s)	2.5
		Cut-out speed, (m/s)	25
		Rated speed, (m/s)	8
		Rated power, (kW)	250
	Enercon E-18	Cut-in speed, (m/s)	2.5
		Cut-out speed, (m/s)	25
		Rated speed, (m/s)	12
		Rated power, (kW)	80
PV modules (1 type) [36]	Canadian solar Hiku 7	Rated power, (W)	665
		Module efficiency, (%)	21.1
		Operating current, (A)	17.28
		Operating voltage, (V)	38.5
		Open circuit voltage, (V)	45.6
		Short circuit current, (A)	18.51
		NOCT, (°C)	42 ± 3
		Temperature coefficient, (%/°C)	−0.26
		Lifetime, (years)	20
MLPE inverter	AC rated	Capacity, (kVA)	48

of the energy system and study its impact on the system's dynamic operation.

Consequently, four main control strategies based on the modification of the traditional rule-based control strategies have been formulated herein. They are, the load following (LF) strategy without battery, load following with battery, circuit charging (CC) without battery and circuit charging with battery. The CC also considers sole and split ST back-ups. The net load, $P_{\mathrm{net}}(\mathrm{t}) = (P_{\mathrm{L}}(\mathrm{t}) - P_{\mathrm{PV}}(\mathrm{t}) - P_{\mathrm{WT}}(\mathrm{t}))$ i.e., the difference between the load and the power generated from the PV and WT generators, the state of charge of the battery (SOC) and the split of the ST are the control parameters that are used for the ON/OFF control of the ST back-up and the discharging and charging of the batteries. To achieve the efficient management of the system, the central controller is expected to check the SOC of the battery and P_{net} at each time step (every 1 h). The other conditions required for the efficient control of the energy system are:

- Uninterrupted energy flow from the PV, WT, battery storage and the main and auxiliary back-up at every time step must be maintained.
- All power generators may operate simultaneously when necessary.
- All excess power generation from the generating units should be dumped via resistive loads when the battery is fully charged to protect the load from over-voltage.
- Battery charging and discharging limits must be maintained to prevent excessive charging and total discharge of the battery.
- When the ST is powered ON, the low grade flue gas should be deployed to produce some cooling and heating.
- To avoid wet expansion in the turbine of the ORC due to low grade waste heat from the ST, the ORC should only be operated when the ST is operating above a minimum threshold.

The rule-based formulations and operational conditions for the storage, generation and dispatch of energy for each of the proposed control strategies are presented in the supplementary materials.

5. Formulation of the optimisation problem

The bi-level optimisation of the energy system has been formulated as a multi-objective problem in the outer-loop that deals with the sizing of the system components. Thus, the optimal system configuration is found by the simultaneous minimisation of the loss of power supply probability (LPSP), levelised cost of energy (LCOE) and dumped power. For a predefined load profile of the consumer, the optimisation problem aims to determine the optimal number of system components, type of components, control strategy and split of the ST back-up that will minimise the levelised cost of energy (LCOE), loss of power supply (LPSP), dumped power (P_{Dumped}) and greenhouse gas (GHG) emissions ($y_{\mathrm{GHG}}^{\mathrm{F}}$) over the plant life of 20 years. This section presents the mathematical formulation of the objective functions and the constraints that must be satisfied to select an optimum system configuration.

5.1. Optimisation function

The formulated evaluation metrics are the mathematical expressions of the objective functions. The optimisation problem is formulated as a

three-objectives function problem aimed at simultaneously minimising the objectives and is presented as follows:

$$minimise\ f(X) = f_i(X), f_j(X), f_k(X)\ \ i \neq j \neq k$$

$$\forall : g_i(X) = 0\ \ and\ \ h_i(X) \leq 0 \tag{11}$$

$$X \in \{X_i, i = 1, 2, \cdots\cdots n - 1, n\} \tag{12}$$

where $i,j,k \in \{1,2,3\}$, the objective functions, $f \in \{\text{LCOE, LPSP, P}_{\text{dumped}}\}$, g_i are the equality constraints, h_i are the inequality constraints and X are the decision variables. X_1 = number of PV modules in parallel, X_2 = number of wind turbines, X_3 = type of wind turbine, X_4 = the capacity of the ST + ORC back-up, X_5 = number of batteries in parallel, X_6 = type of battery, X_7 = number of split and X_8 = control strategy.

The objective functions are formulated as follows:

(i) Levelised cost of energy

The levelised cost of energy (LCOE) is the unit cost of the energy produced from the system over its life cycle. It is the ratio of the net present cost (NPC) of the generating power from the system to the total electricity demand [37]. The NPC comprises the installation and acquisition cost of the components, the operating and maintenance (O&M) cost, the replacement cost of components, and the cost of fuel for the entire life of the system converted back to the initial time of purchase of the components (year 1). Considering the interest and inflation rates, the NPC can be expressed as [28,29]:

$$NPC = \sum_j \left(Annc_{I\&A,j} + Annc_{O\&M,j} + Annc_{rep,j} + Annc_{fuel,j} + Annc_{start-up,j} \right),$$

$$j \equiv PV, WT, Bat, ORC, ST, Inv \tag{13}$$

where the annualised acquisition and installation cost, $Annc_{I\&A}$, annual operating and maintenance cost, $Annc_{O\&M,j}$, annual replacement cost, $Annc_{rep,j}$, annual fuel cost, $Annc_{fuel,j}$, and annual start-up cost, $Annc_{start-up}$, respectively of a component, j are given by [38 28,29]:

$$Annc_{I\&A} = \sum_j C_{I\&A,j} \times N_j \tag{14}$$

$$Annc_{O\&M} = \sum_{i=1}^{n_{system}} C_{O\&M,j} \left(\frac{(1 + r_{inf})^{n_{system}}}{(1 + r_{int})^{n_{system}}} \right) \tag{15}$$

$$Annc_{rep} = \sum_{m=1}^{N_{rep,j}} C_{I\&A,j} \left(\frac{(1 + r_{inf})^{m.n_j}}{(1 + r_{int})^{m.n_j}} \right) - C_j \left(\frac{n_j - (n_{system} - N_{rep,j}n_j)}{n_j} \right) \left(\frac{(1 + r_{inf})^{n_{system}}}{(1 + r_{int})^{n_{system}}} \right) \tag{16}$$

$$Annc_{fuel,j} = \sum_{i=1}^{n_{system}} C_{fuel,j} \left(\frac{(1 + r_{inf})^{n_{system}}}{(1 + r_{int})^{n_{system}}} \right) \tag{17}$$

$$C_{start-up,j} = \sigma_j + \delta_j \left[1 - exp\left(\frac{-T_{off,j}}{\tau_j} \right) \right] \tag{18}$$

where $N_j(-)$ is the number of components j, $C_{I\&A,j}(\$)$ is the installation and acquisition cost, $C_{O\&M,j}(\$)$ is the operating and maintenance cost, $N_{rep,j}(-)$ is the number of replacements of component j, $C_{fuel,j}(\$)$ is the cost of fuel, $n(-)$ is the life of the component or system, $r_{inf}(\%)$ is the

Table 3
Key system components cost and other assumptions.

Component	Description	Value
Acquisition and installation cost		
Wind turbine	Enercon E-18 per kW (US $)	700 [40]
	EWT DW 52–250 per kW (US $)	700 [40]
Solar PV	Hiku 7 cost per panel (US $)	987 [36]
Battery	Hoppecke 620 Ah (US $)	350 [35]
	Hoppecke 890 Ah (US $)	405 [35]
	Hoppecke 1120 Ah (US $)	530 [35]
Stirling engine	Acquisition cost per kW (US $)	500 [41]
ORC engine	Acquisition cost per kW (US $)	1700 [42]
MLPE inverter	Cost per kW (US $)	120 [40]
Operating and maintenance cost		
Fuel cost	Nigerian woodchips (US $)	85
Wind turbine	Maintenance cost per kW (US $)	0.02 [43]
PV	Maintenance cost per kW (US $)	0.005 [43]
Stirling engine	Maintenance cost per kW (US $)	0.0095 [41]
ORC engine	Maintenance cost per kW (US $)	0.008 [42]
Financial assumptions		
Interest rate	Bank interest rate on capital (%)	12.5
Inflation rate	Inflation rate on capital (%)	15
Battery life	Life span of battery (years)	7
Plant life	Life span of the system (years)	20

inflation rate, $r_{int}(\%)$ is the interest rate, σ_j is the hot start-up cost of the engine, cold start-up cost of the engine, T_{off} is the period of engine shut down and τ_j is the constant for engine cooling time.

The cost of fuel, $C_{fuel,j}$ is given as:

$$C_{fuel} = \left\{ c_{fuel} \sum_{t=0}^{8760} FC_{ST+ORC}(t) \right. \tag{19}$$

where $c_{fuel}(\$/kg)$ is the unit cost of the fuel. The levelised cost of energy is therefore given as [39]:

$$LCOE = \frac{NPC}{\sum_{t=1}^{t=8760} P_L(t)} \tag{20}$$

The cost data of the components and other financial assumptions used to evaluate the economic objective in this study are provided in Table 3.

(ii) Loss of power supply probability

The loss of power supply probability (LPSP) is a statistical parameter that assesses the reliability of the renewable energy resources in meeting the electricity demand of the design location. It is also a measure of the renewable fraction of the system. Low LPSP connotes high renewable

fraction and reliability of the energy system. The LPSP has been expressed as follows [37,39]:

$$LPSP = \frac{\sum_{t=1}^{t=8760} \left(P_L(t) - (P_{PV}(t) + P_{WT}(t)) + P_{ST+ORC}(t) + P_{Bat,SOC^{min}} \right)}{\sum_{t=1}^{t=8760} P_L(t)} \tag{21}$$

(iii) Dumped power

The dumped power quantifies the amount of excess electricity being generated by the HRES that is dumped via resistive loads. The generation of excess power is inevitable in a HRES because PV and WT power generation is at variance with the electricity consumption. Hence, excess

power is generated from the HRES, which indicates that the system is over-sized and this results in high energy cost. On the other hand, power curtailment with the intention of reducing dumped power, results to high energy cost and increased emissions, because of the increased reliance on the back-up to augment the load. It is therefore, important to minimise the dumped power from the renewable generators in a HRES, while simultaneously minimising the deployment of the back-up. The dumped power from the HRES can be obtained as follows:

$$P_{Dumped} = \begin{cases} \sum_{t=1}^{t=8760} \left((P_{PV}(t) + P_{WT}(t)) - P_L(t) \right), (P_{PV}(t) + P_{WT}(t) > P_L(t) \\ (P_{ST+ORC}(t) - P_L(t)), P_{ST+ORC}(t) > P_L(t) \end{cases}$$

(22)

5.2. System design and operating constraints

The optimal solution must satisfy the following conditions:

(i) Energy generation and consumption matching: This constraint ensures that at every time step, the total generation from renewable generators and the back-up match with the load and power stored in the battery or dumped via resistive loads.

$$P_L(t) + P_{ch,Bat}(t) + P_{dumped}(t) \le P_{ST+ORC}(t) + N_{PV}P_{PV}(t) + N_{WT}P_{WT}(t) + P_{disch,Bat}(t)$$

(23)

(ii) Back-up power limits: hourly power generation from the back-up shall not exceed these limits,

$$P_j^{min} \le P_j(t) \le P_j^{max}, j = ST \ or \ ORC$$

(24)

(ii) Battery storage and discharge limits: the maximum depth of discharge (DOD) of the battery has been furnished by the manufacturer. In this study, the battery is only expected to discharge power when its capacity is above SOC_{min}. By contrast, in the charging mode, the power stored in the battery is not expected to exceed SOC_{max}.

$$(1 - DOD)\left(\frac{N_{Bat}}{N_{Bat,S}}\right)C_{Bat,max} \le C_{Bat}(t) \le \left(\frac{N_{Bat}}{N_{Bat,S}}\right)C_{Bat,max}$$

(25)

where $N_{Bat}(-)$ is the total number of batteries, $N_{Bat,S} = \frac{V_{Bus}}{V_{Bat}}$ is the number of batteries in series, $V_{Bus}(V)$ is the bus voltage, $C_{Bat,max}(Ah)$ is the maximum capacity of the battery. Furthermore, the power stored in the battery or discharged from the battery must not exceed the capacity of the battery.

$$\text{Battery discharge mode}: P_{disch,Bat}(t) \le \left(\frac{N_{Bat}}{N_{Bat,S}}\right)C_{Bat,max}V_{Bat}$$

(26)

$$\text{Battery charge mode}: P_{ch,Bat}(t) \le \left(\frac{N_{Bat}}{N_{Bat,S}}\right)C_{Bat,max}V_{Bat}$$

(27)

(iii) Battery capacity: here the battery storage has been designed to handle mainly the constant base load demand in the morning and the transient load at peak hours. Hence, a constraint to ensure the battery capacity is sufficient to match the base load when it is in the power discharge mode has been introduced into the system sizing optimisation:

$$\text{Battery capacity}: N_{Bat}.C_{Bat,max} \ge z_f P_L$$

(28)

where $z_f(-)$ is the battery capacity factor.

(iv) Limits on components: upper and lower limits have been set on the number of components and types of components. In the case of the type of components, the absolute value of the random number generated within the given range represents the type of the component, j selected and this will prompt the release of the corresponding component data.

$$X_{j,min} \le X_j \le X_{j,max}$$

(29)

where $X_{j,min}(-)$ is the lower bound, $X_{j,max}(-)$ is the upper bound and $X_j(-)$ is the number or type of component, j. The range of values of the decision variables are given in Table 4. These range of values are selected considering the constraint on land availability and other economic and environmental considerations.

5.3. Bi-level optimisation solution method

The solution approach for the bi-level optimisation performed in this paper to determine the optimal size of the components of the HRES system, by integrating the system sizing optimisation and the control strategy is presented in this section. The modified non-dominated sorting genetic algorithm (NSGA-II) has been deployed to solve the formulated optimisation problem. Further, the solution of the GA is utilised as initial guess for a secondary optimizer to ensure that the local optimum of the global optimum neighborhood is identified. In the past, GA algorithms have used for bi-level sizing optimisation of similar systems and in particular in the outer-loop to determine the optimum number of the system components. The details of the GA operators are presented in Table 5. These values are ideal for obtaining good results and have been deployed in Ref. [25].

In Fig. 3, the algorithm for implementing the multi-objective optimisation has been represented. As seen in Fig. 3, it starts by generating the initial cluster of possible solutions to the optimisation problem, which is a set of combinations of the component types, number and capacity including the control strategy and number of split of the ST. The initial population of individuals, Pop_i in the first generation, G_i, comprises n different configurations of the HRES that will be evaluated to determine the configuration that best minimises the LPSP, LCOE and dumped power, after several generations. The initial population, Pop_i is represented in a vector form as:

Table 4
The upper and lower bounds of the decision variables.

Parameter	Lower bound	Upper bound
Number of PV in parallel	1	1200
Number of type 1 wind turbine	0	5
Number of type 2 wind turbine	0	8
Wind turbine type	1	2
ST + ORC capacity	140	220
Number of batteries in parallel	1	30
Battery type	1	3

Table 5
Specifications of the GA operator.

Parameter	Value
Population size	250
Population type	Double vector
Pareto fraction	0.5
Maximum generation	500
Cross-over operator	Intermediate
Cross-over fraction	0.8
Mutation rate	0.01
Hybrid function	fgoalattain
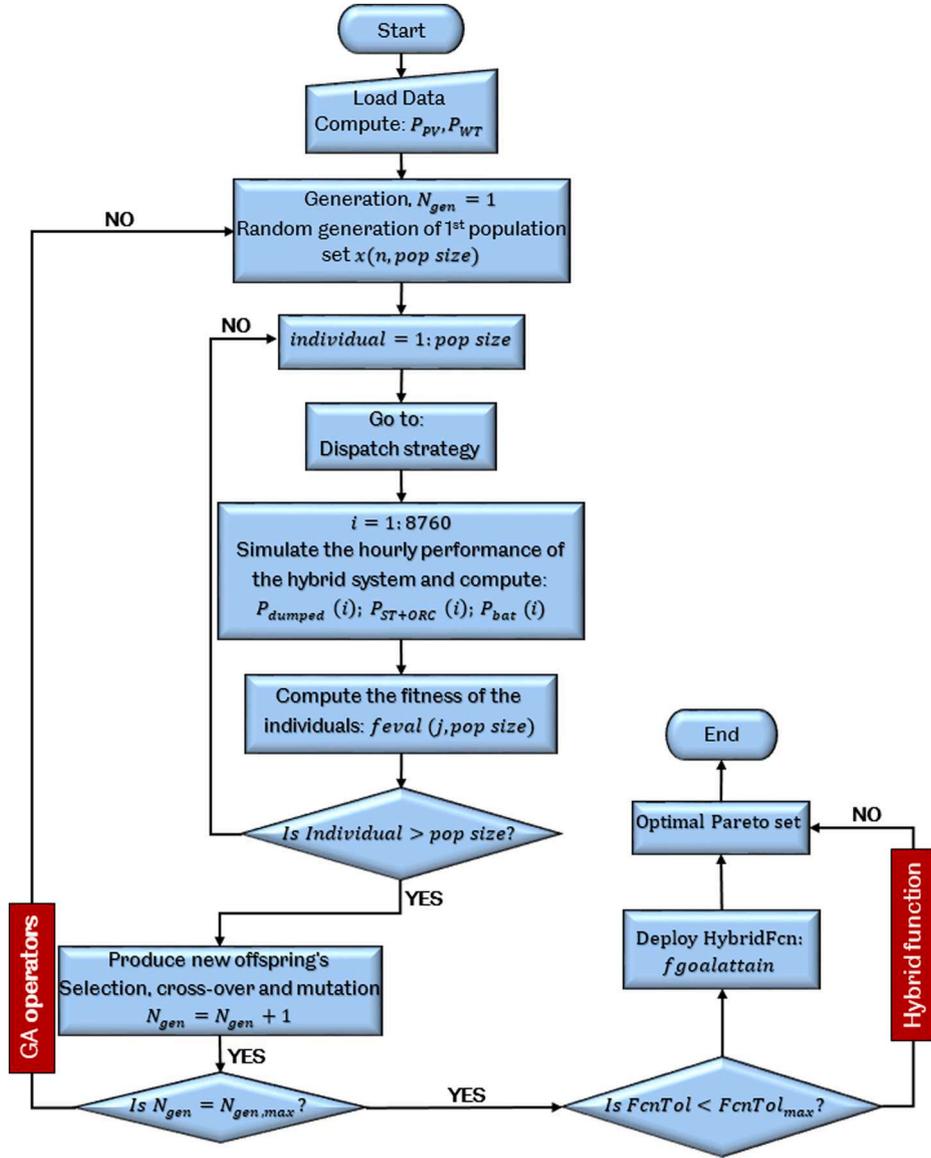
Fig. 3. Algorithm for the simulation and optimisation of the energy system based on genetic algorithm.

$$Pop_i = \begin{bmatrix} X_1^1 X_2^1 X_3^1 X_4^1 X_5^1 X_6^1 X_7^1 X_8^1 \\ X_1^2 X_2^2 X_3^2 X_4^2 X_5^2 X_6^2 X_7^2 X_8^2 \\ X_1^3 X_2^3 X_3^3 X_4^3 X_5^3 X_6^3 X_7^3 X_8^3 \\ \dots \\ \dots \\ \dots \\ \dots \\ X_1^n X_2^n X_3^n X_4^n X_5^n X_6^n X_7^n X_8^n \end{bmatrix} = \begin{bmatrix} X_1 \\ X_2 \\ X_3 \\ . \\ . \\ . \\ . \\ X_n \end{bmatrix} \qquad (30)$$

where X is a vector representing the genotype of each individual in the population.

Fig. 4 illustrates the interconnection between the HRES sizing optimisation and the implementation of the control strategy. As it is evident from Fig. 4, the control parameters, $x_k \ni (P_{net}(t), SOC(t), u_j, u_k)$ are sent to the inner-loop to simulate the hourly energy dispatch for a given control strategy, $u_j \in (1, 4)$ as described previously. Then, the computed output signals including the power supplied by the ST + ORC and battery are relayed to the outer-loop at the end of one year, ($t = 8760$), to

compute the objective functions. This step is repeated for all the individuals in the population, then the optimisation operators are deployed to generate the next generation of individuals.

These iterative steps are performed until the stopping criteria is met. The optimal system configuration, $X^{best} = [X_1^{best} X_2^{best} X_3^{best} X_4^{best} X_5^{best} X_6^{best} X_7^{best} X_8^{best}]$ is selected from the Pareto set of non-dominated solutions by deploying the TOPSIS decision making tool.

Finally, the hourly performance of the optimal HRES configuration for each control strategy is simulated by deploying the algorithms already described. The implementation of the optimisation and dynamic simulation have been performed in MATLAB. A connection was made between MATLAB and Aspen plus environment as described in a previous work done by the authors in Ref. [31], to control the operation of the Aspen models of the thermal chiller, ORC, boiler and the drying and combustion of the woodchips fuel. However, the models for the prediction of the generation from the PV and WT have been built in Simulink and the input weather and load data of the test location have been linked to the ports of the Simulink block from Excel spreadsheet.
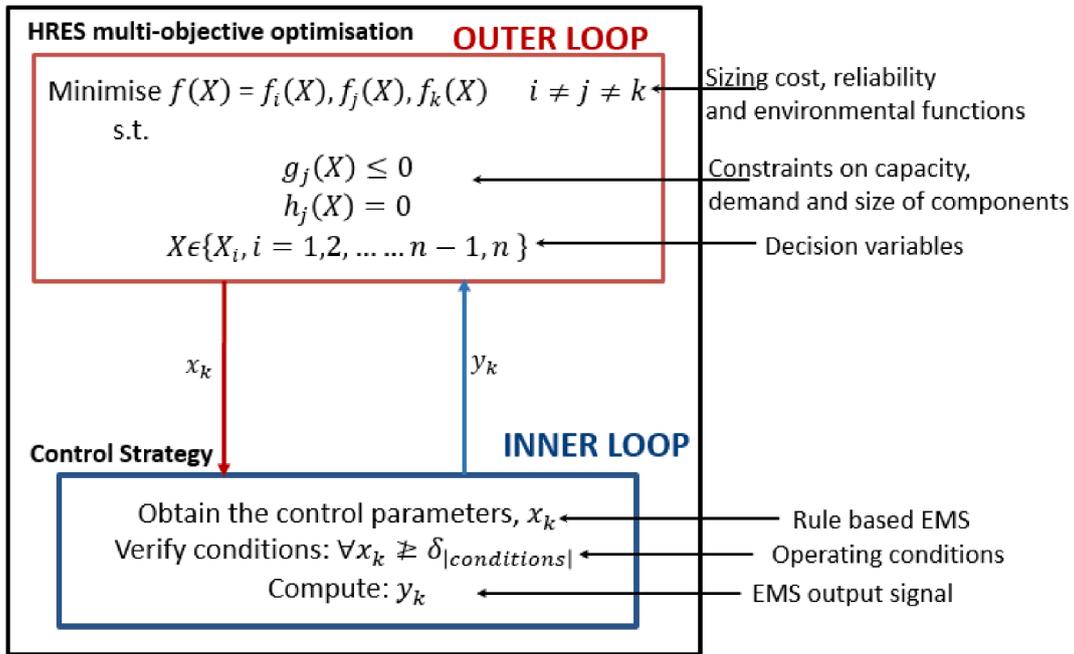
Fig. 4. Algorithm for the bi-level optimisation of the HRES and EMS.
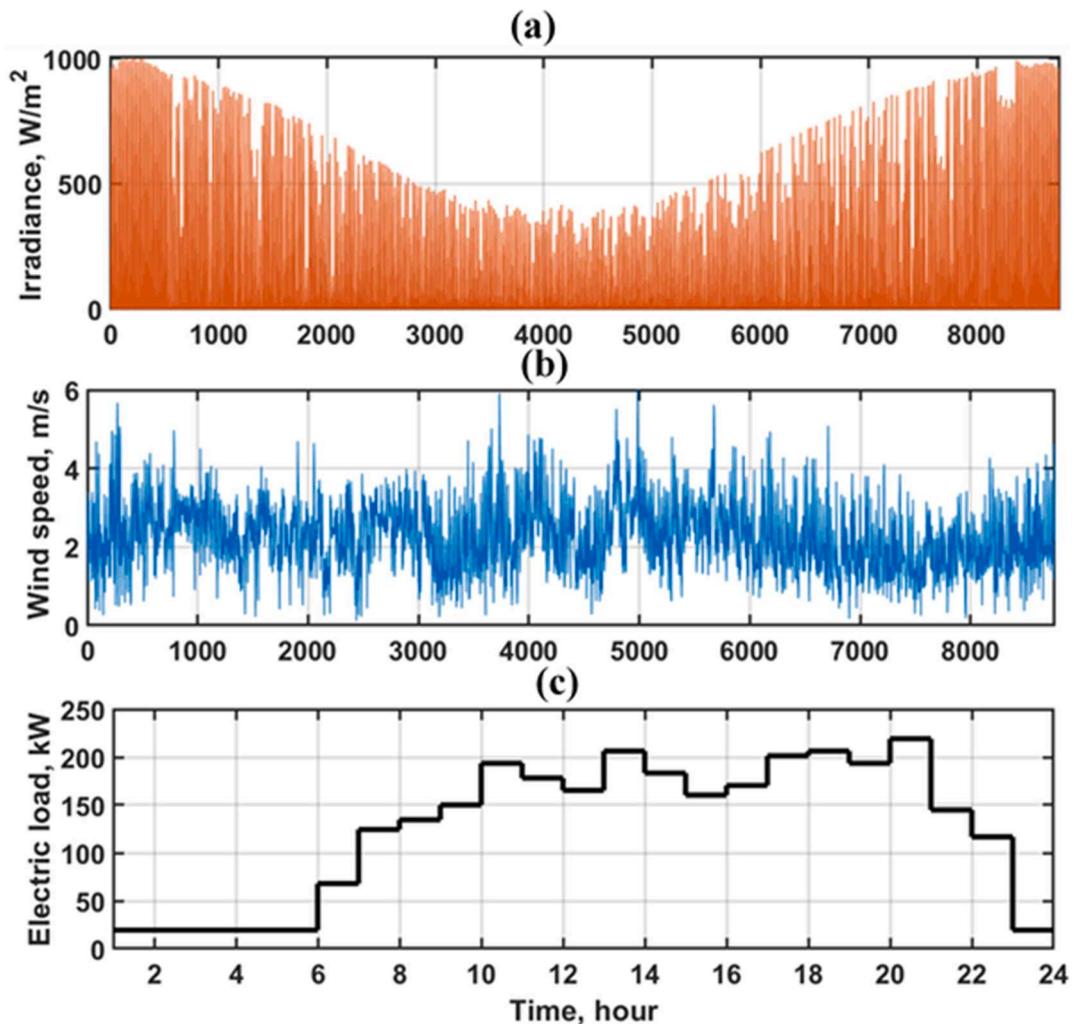
Fig. 5. Weather and load data of the test location [44,30].
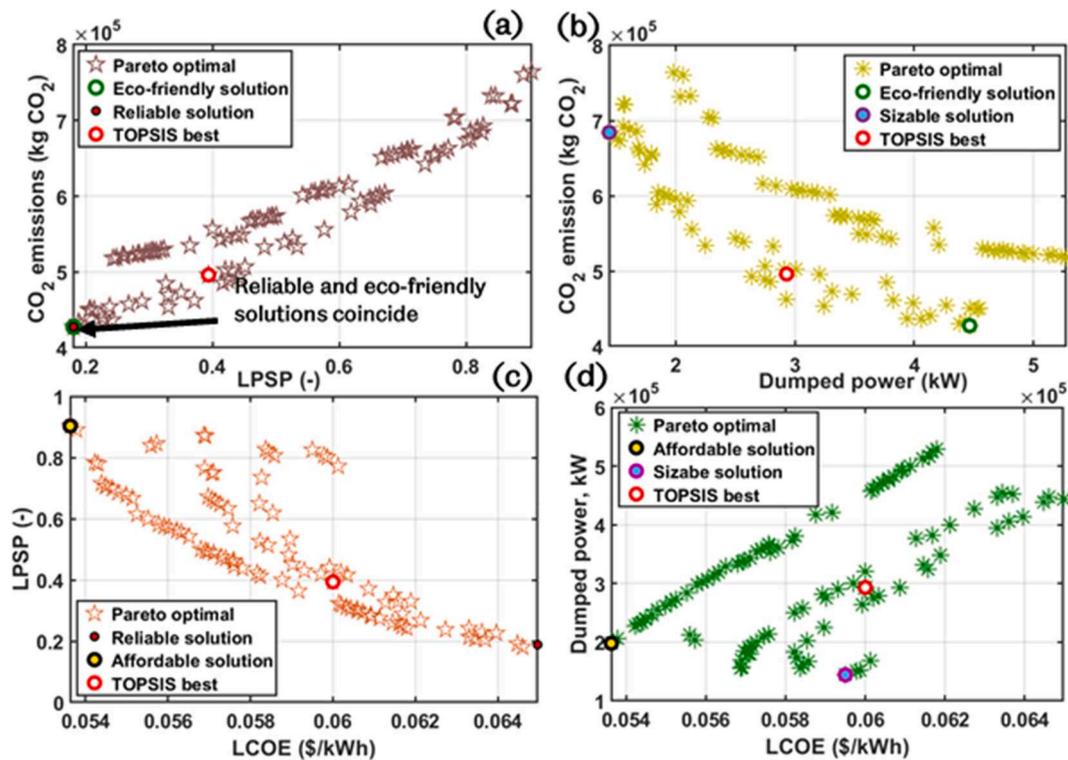
Fig. 6. Pareto optimal solutions obtained from the bi-level optimisation of the energy system.

Table 6
Results of optimal system configuration of HRES components for different control strategies.

Control strategy	1	2	3	4
LCOE (cent/kWh)	5.835	6.08	9.09	6.32
LPSP (-)	0.4074	0.3962	0.8924	0.3801
Dumped power (MWh)	385.10	287.8	987.4	337.3
Number of PV	4 × 982	4 × 934	4 × 1032	4 × 982
Wind Turbine type	EWT 52–250	EWT 52–250	EWT 52–250	EWT 52–250
Number of WT	4	5	5	5
Battery Type	–	Type 2	–	Type 3
Number of batteries	–	4 × 26	–	4 × 30
Capacity of ST + ORC (kW)	180	193	180	180
Annual PV power (MWh)	723.53	688.16	760.37	723.53
Annual WT power (MWh)	264.21	330.26	330.26	330.26
Annual ST + ORC power (MWh)	408.81	361.71	937.50	387.50
CO_2 emissions (kg CO_2)	0.542 × 10^6	0.479 × 10^6	1.291 × 10^6	0.5140 × 10^6

6. Results and discussion

The bi-level system sizing and control strategy optimisation have been implemented in MATLAB on a 16.0 GB four cores Intel Xeon computer with the weather and load data obtained from a test location. The test location is a remote location in Southern Nigeria with total electricity demand of 2.952 MWh/day. Fig. 5 presents the hourly local weather data of global solar irradiance and wind speed and the load demand of the test location [30,44]. The location's solar irradiance varies between 150 W/m^2 to 1000 W/m^2, while the wind velocity measured at 10 m hub height indicates an average speed of 3.0 m/s as seen in Fig. 5 (a) and (b), respectively. Also, the peak load in the test

location is 210 kW and it is observed at the 19 h in the day as seen in Fig. 5 (c).

The optimal system configuration and control strategy that minimise the LPSP, LCOE and dumped power have been obtained after 150 generations of the GA. The computing speed of the optimisation problem has been enhanced by deploying parallel computing and it converged in 26.68 min. Fig. 6 shows the Pareto optimal solutions obtained from the bi-level multi-objective optimisation of the HRES sub-system of the integrated multi-carrier system. The conflicting nature of the multi-objective problem is evidenced from the high degree of scatter in the Pareto front. It is further demonstrated by the trend in the Pareto optimal solutions presented in Fig. 6, and this is expected particularly for a bi-level multi-objective optimisation problem integrating component sizing with the EMS optimisation. It can be seen that, the LPSP exhibits a direct relationship with the CO_2 emitted from the system, i.e., high renewable energy penetration yields reduced emissions, while the latter is inversely correlated to the dumped power because of the periodic nature of renewable generators. On the other hand, low LCOE coincides with high LPSP and vice versa, whereas the former enjoys a positive relationship with the dumped power.

Also, the ideal solutions from the perspective of reliability, eco-friendliness, compact size and affordability have been featured in Fig. 6. It is clear from these results that, no single solution satisfies all the four objectives equally. Hence, TOPSIS decision making tool has been deployed to obtain the best configuration in each case as highlighted in Fig. 6 and the corresponding configurations of the TOPSIS best optimal system for each control strategy have been specified in Table 6. The TOPSIS best evidently ensures a reasonable trade-off in the objectives. As has been previously mentioned, in this study, control strategy 1 is load following without batteries, control strategy 2 is load following (LF) with battery, control strategy 3 is circuit charging (CC) without battery and control strategy 4 is circuit charging with battery.

It can be noticed in Table 6 that, the optimal configuration obtained for control strategy 2 deploys the least number of renewable generators (PV and WT) to fulfill the load and generates 688.16 MWh and 330.26 MWh of solar and wind power, respectively. On the contrary, the

Table 7
Results of optimal system configuration of HRES with the deployment of split ST in control strategy 3.

Number of split	1 (Ctr 3)	2 (Ctr 3a)	4 (Ctr 3b)
LCOE (cent/kWh)	9.09	7.26	6.39
LPSP (-)	0.8924	0.6682	0.5378
Dumped power (MWh)	987.4	632.9	471.8
Number of PV	4×1032	4×964	4×944
Wind Turbine type	EWT 52–250	EWT 52–250	EWT 52–250
Number of WT	5	5	5
Battery Type	–	–	–
Number of batteries	–	–	–
Capacity of ST + ORC (kW)	180	180	180
Annual PV power (MWh)	760.37	710.26	695.52
Annual WT power (MWh)	330.26	330.26	330.26
Annual ST + ORC power (MWh)	937.50	673.04	522.70
CO2 emissions (kg CO_2)	1.291×10^6	0.894×10^6	0.693×10^6

Table 8
Results of optimal system configuration of HRES with the deployment of split ST in control strategy 4.

Number of split	1 (Ctr 4)	2 (Ctr 4a)	4 (Ctr 4b)
LCOE (cent/kWh)	6.32	6.131	6.144
LPSP (-)	0.3801	0.3978	0.3929
Dumped power (MWh)	337.3	323.5	320.0
Number of PV	4×982	4×959	4×965
Wind Turbine type	EWT 52–250	EWT 52–250	EWT 52–250
Number of WT	5	5	5
Battery Type	Type 3	Type 2	Type 2
Number of batteries	4×30	4×29	4×29
Capacity of ST + ORC (kW)	180	186	190
Annual PV power (MWh)	723.53	703.70	711.00
Annual WT power (MWh)	330.26	330.26	330.26
Annual ST + ORC power (MWh)	387.50	393.99	361.52
CO2 emissions (kg CO_2)	0.514×10^6	0.523×10^6	0.504×10^6

optimal system configuration in CC without battery storage utilises the most number of PV generators and generates 760.37 MWh and 330.26 MWh of PV and wind power, respectively. Regarding the deployment of battery storage, if the optimal system configuration in control strategy 1 is compared to that in control strategy 2, it is notable that the total power generated by the renewable generator in the latter exceeds the former by 30.68 MWh. However, the former deploys the ST + ORC back-up more and consumes 47.1 MWh more power from the back-up compared to the LF with battery. The higher power generation from the renewable generator in control strategy 2 compared with control strategy 1 is driven by the need to store excess power in the batteries and minimise the utilisation of the ST + ORC back-up. Consequently, the LPSP, LCOE, dumped power, CO_2 emissions obtained in control strategy 2 is lower when compared with control strategy 1. The dumped power, CO_2 emissions and LPSP reduce by 25.3%, 11.62%, 2.75%, respectively, while the LCOE increases by 4.18%, with the deployment of battery storage in load following.

Conversely, it is evident from the optimal system configuration obtained in CC mode that, the inclusion of batteries to store excess power generated from the dispatchable and non-dispatchable units (control strategy 4), reduces the capacity of the generators compared to the case of CC without battery (control strategy 3). A huge difference in the power delivered by the ST + ORC back-up of 550 MWh (58.6% higher) in control strategy 3 compared with control strategy 4 is remarkable. This is because the ST + ORC back-up operates at its rated capacity in CC mode and the absence of BSS in control strategy 3 suggests that the excess power generated in its operation will all be dumped. Additionally, the absence of BSS results to more frequent deployment of the ST + ORC back-up in this EMS strategy. Consequently, the LCOE, LPSP, and CO_2 emissions of the optimal system in control strategy 3 drastically reduce by 30.47%, 57.41%, and 60.18% with the deployment of BSS in
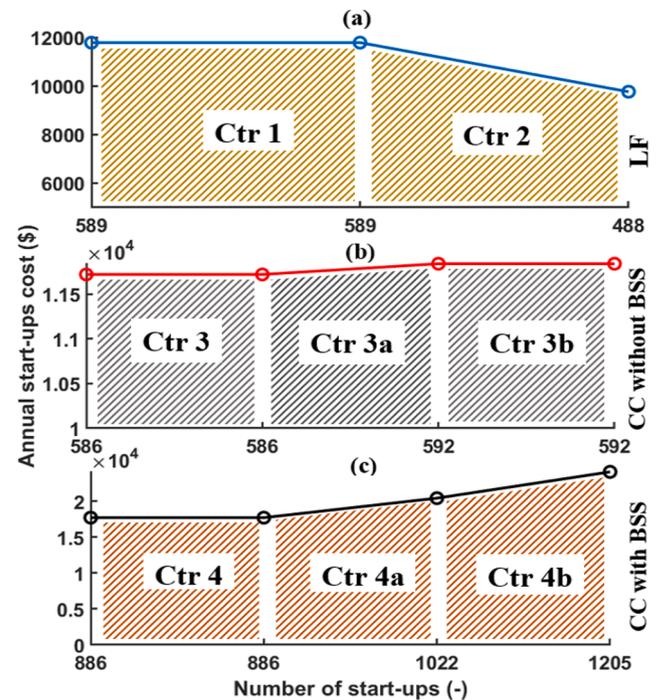
Fig. 7. Start-up frequency and costs from the back-up in the control strategies.

control strategy 4. It is evident that with the inclusion of battery storage in the optimal system, the renewable generators compared to the system without BSS, particularly in the LF mode, generate lesser power. Finally, the optimal configuration in control strategy 2 (load following with battery) offered the lowest LCOE, LPSP, dumped power and CO_2 emissions.

Table 7 and Table 8 present the results of the optimal system configurations obtained with the deployment of two and four-split ST cases in control strategies 3 and 4, respectively. Here, deploying two-split ST and four-split ST in control strategy 3 have been represented by (Ctr 3a) and (Ctr 3b), respectively, while deploying two-split ST and four-split ST in strategy 4 are represented as (Ctr 4a) and (Ctr 4b), respectively. As can be seen in Table 7, the number of components of the renewable generators and BSS and the generation capacity of the ST + ORC back-up reduce with the increase in the number of splits deployed in CC without battery (control strategy 3) [11].

Consequently, the LCOE, LPSP, dumped power and CO_2 emissions decline with the increase in the number of splits. The most remarkable reductions are seen in the dumped power that records 30.75% and 35.9% decrease and CO_2 emissions with observed decrease of 46.32% and 52.22%, with the deployment of 2-split ST and 4-split ST, respectively. Therefore, the deployment of split ST reduces the capacity of the system and significantly improves its global performance in circuit charging without battery.

Similarly, when batteries are deployed to store the excess power generated by the renewable generators in control strategy 4, the deployment of split ST reduces the dumped power with the increase in the number of splits. Further, the deployment of 2-split ST in Ctr 4a reduces the LCOE slightly, but contrary to the claim in the literature [11] and the findings in CC without battery storage, further reduction in the LCOE is not seen with the deployment of 4-split ST [12]. As it is noticeable in Fig. 7 that represents the annual start-ups of the back-up and the associated costs, the number of start-ups in CC with BSS increases with the increase in the number of split.

There were 1205 start-ups when 4-split ST is deployed, which is 183 and 319 start-ups more than when 2-split and 1-big ST are deployed, respectively. By comparison, the number of start-ups in CC without BSS increases slightly from 586 to 592 with the deployment of 2-split ST but
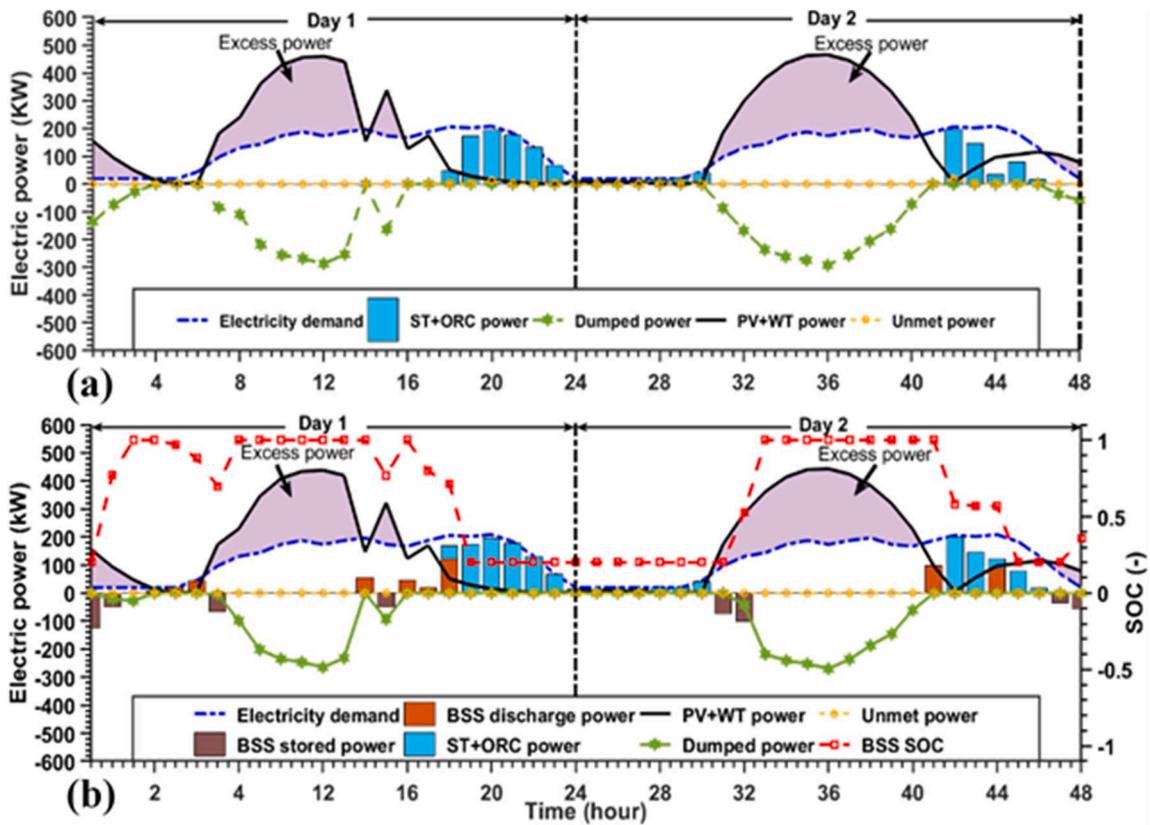
Fig. 8. Hourly commitments of system units in fulfilling customer electricity demand by the load following mode (a) without battery and (b) with battery.
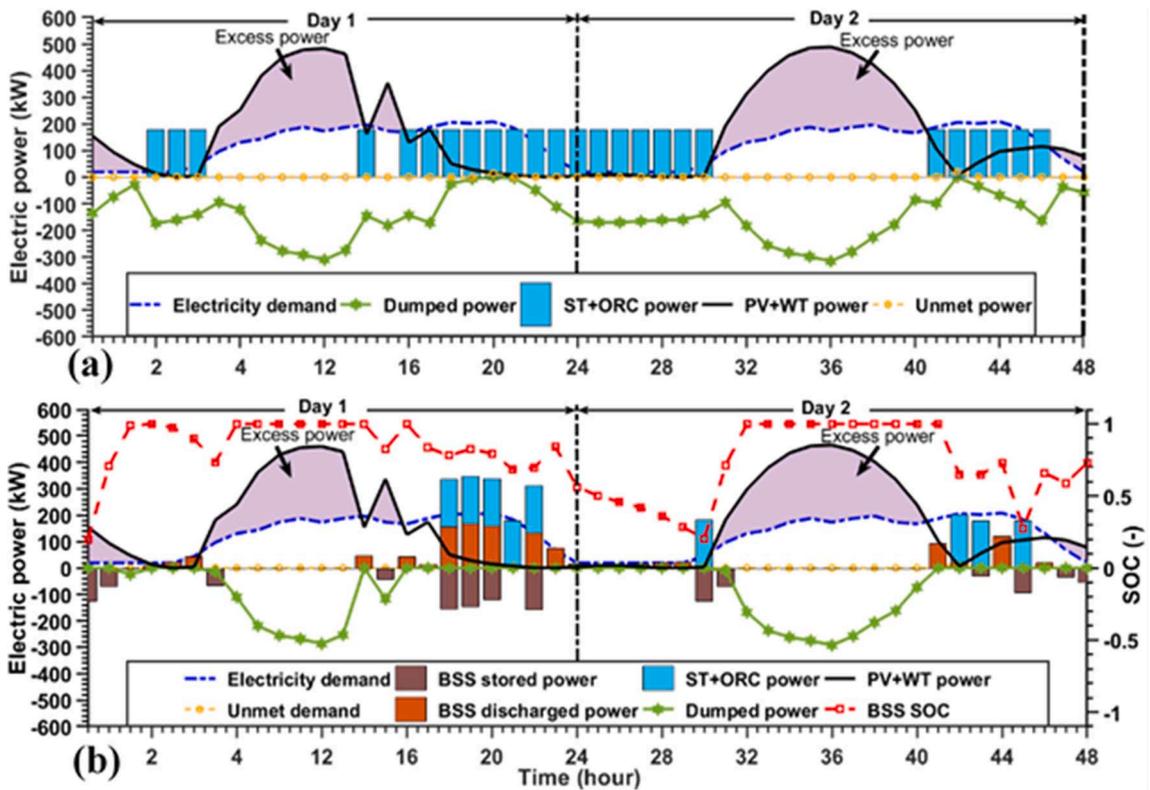
Fig. 9. Hourly commitments of system units in fulfilling customer electricity demand by the circuit charging mode (a) without battery and (b) with battery.

did not change with further increase in the number of splits. On the other hand, in the LF, the inclusion of BSS reduces the number of start-ups, because the battery will be deployed a few times, minimising the dependence on the back-up.

On the contrary, the inclusion of batteries produce an opposite effect in CC with BSS, because of the dual role of the ST + ORC back-up in this case. Therefore, as the commitment of the ST to fulfilling the net load reduces with the increase in the number of splits in Control strategy 4, its capacity to charge the batteries reduces. Consequently, there will be more start-ups and corresponding increase in the running cost of the system which is responsible for the slight increase in the LCOE. Nevertheless, the LCOE in Ctr 4b is still lower than Ctr 4 that uses one big ST, because of the fewer components deployed in the former and significantly reduced deployment of ST + ORC back-up (15.9 MWh less) [12]. Further, the CO_2 emissions and LPSP decline with the deployment of 4-split ST in Ctr 4b but increase slightly when 2-split ST is deployed compared to 1-big ST case [12]. Thus, the deployment of 4-split ST improves the system performance slightly in this case but introduces some augmented start-up costs.

6.1. Influence of rule-based EMS on MDES electricity generation and consumption

Several rule-based EMS strategies have been proposed in this study to coordinate the generation, storage and dispatch of energy from the units of the system. This section presents the results of the simulations of the hourly electricity generation and storage of the optimal system configurations in the proposed strategies, for two consecutive days with slightly different weather conditions. The hourly commitment of the programmable and non-programmable units of the energy system towards the fulfillment of the electric load of the energy consumers in the test location are presented in Fig. 8 and Fig. 9 for the LF and CC control strategies, respectively. The optimal system configuration found from the bi-level optimisation vary for all the control strategies as observed in Table 6.

Simulations are presented on a 48 h timespan and it is noticeable that Day 1 is characterised by an extended period of generating activities by the renewable generators (20 h of generation). On the other hand, Day 2 did not show much prospects for generation from the WT in the morning (0 h − 6 h) and could be representative of a day with a low wind speed. Based on the frequency of start-ups of the back-up, battery storage limits

and the dumped power, the following striking points are noted:

- The LF approach limits the frequency of start-ups of the ST + ORC back-up, contrary to the claims in [13]. The CC mode (Fig. 9) requires four start-ups of the back-up to fulfil the load, which is double the number in the LF mode (Fig. 8) and this will result in high system operational cost in this EMS mode. It is seen that the green generators did not generate any power from the 22 h in the first day to the 6 h in the next day. This long period of inactivity of the green generators forced the system to rely on the battery and back-up. However, unlike in CC that the back-up goes through a cycle of start-up and shut-down with the battery, in LF, once the battery is discharged, the ST + ORC back-up simply follows the load minimising the number of start-ups

- The utilisation of BSS to store the excess power from the non-programmable generators reduces the dumping of power in the LF and CC EMS modes (Fig. 8 and Fig. 9). The worst case of power dumping occurs in the CC without battery, where the ST + ORC back-up operates at its rated capacity when in operation. Consequently, the programmable power block contributed to the dumping of power since it operates at the rated capacity while fulfilling the load, unlike in the LF without battery where it simply follows the load.

- The cumulative power handled by the battery, i.e., stored and discharged power and the energy flux have been presented in Fig. 10 for control strategies 2 and 4, where batteries are included in the optimal system configuration. It can be observed that the BSS is more active in the CC dispatch mode as evidenced by the high cumulative power of 1.4 MWh handled by the battery, which is 0.35 MWh more than in the LF mode. However, the BSS experiences many cycles of charging and discharging in CC mode, particularly in the second day marked by low generation from the WT and PV. These many cycles of charging and discharging may result to high wear of the batteries [13,45]. Nevertheless, similar storage and discharge limits are indicated by the BSS for both dispatch strategies.

- Regarding the use of the ORC to supply the unmet power when the ST back-up is operational, the trend of the commitment of ST and ORC is presented in Figs. 11–14. The ORC is deployed only six times in control strategy 2 (Fig. 11 (b)), because the ST back-up is forced to follow the load. Consequently, the quality of the waste heat is inadequate most times to power the bottoming cycle, which helps to reduce the operating cost of the system. On the contrary, with the
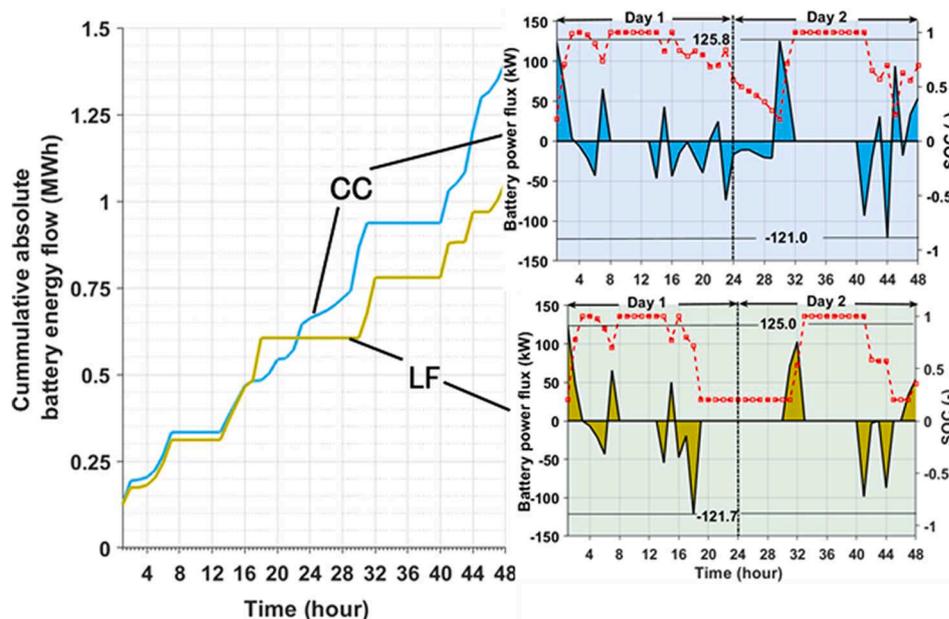
Fig. 10. Hourly energy flow through the batteries for different control strategies.
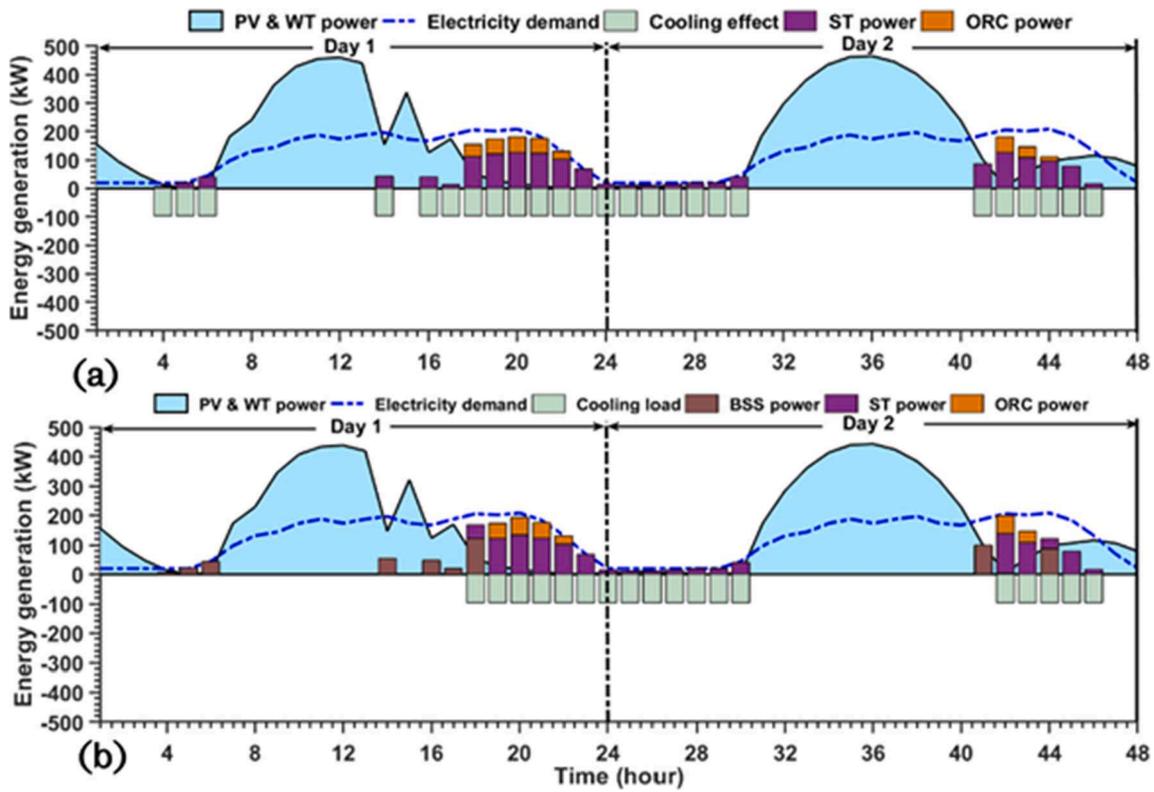
Fig. 11. Hourly generation of cooling and commitment of the dispatchable generators in load following (a) without battery and (b) with battery.
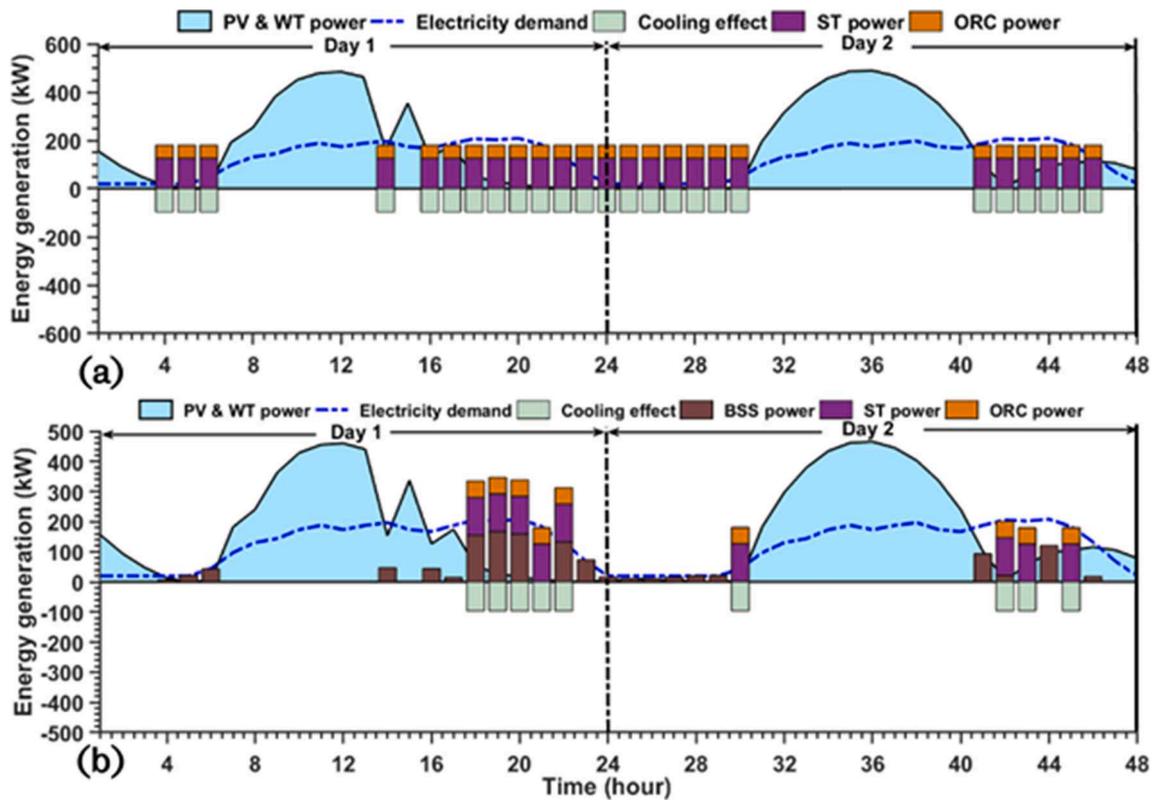
Fig. 12. Hourly generation of cooling and commitment of the dispatchable generators in circuit charging (a) without battery and (b) with battery.
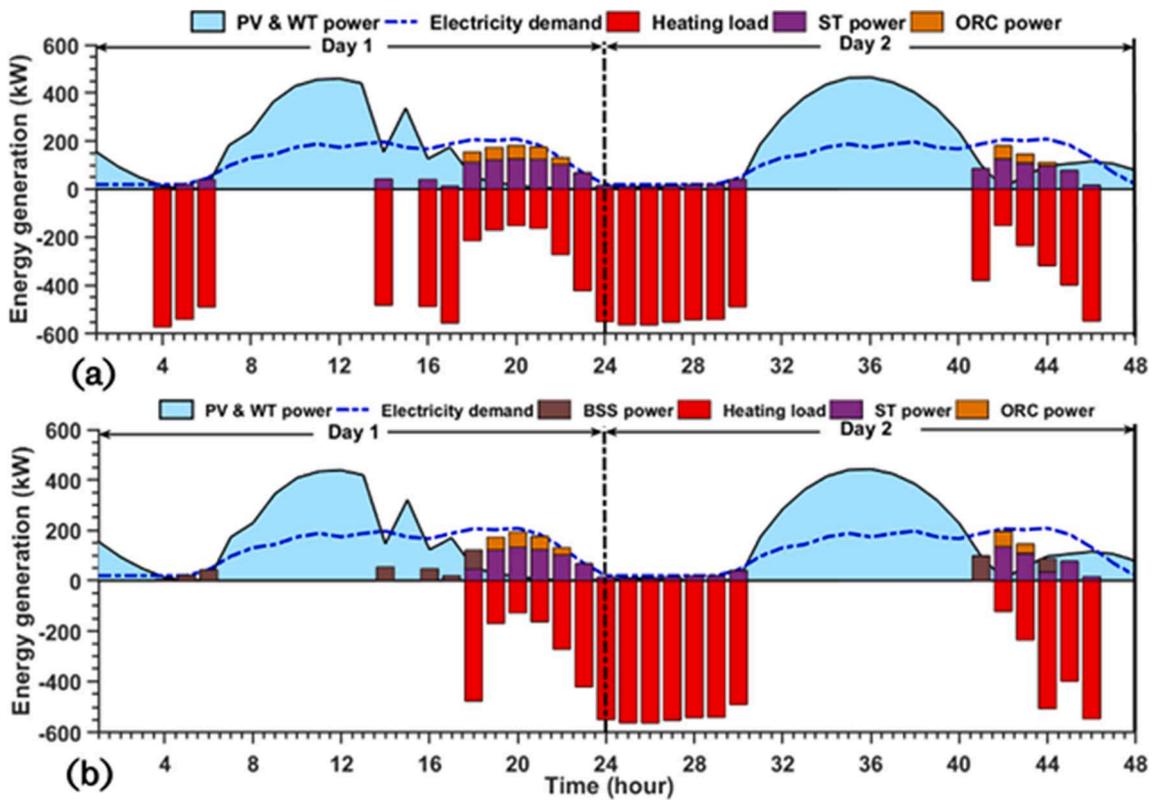
Fig. 13. Hourly generation of heating and commitment of the dispatchable generators in load following (a) without battery and (b) with battery.
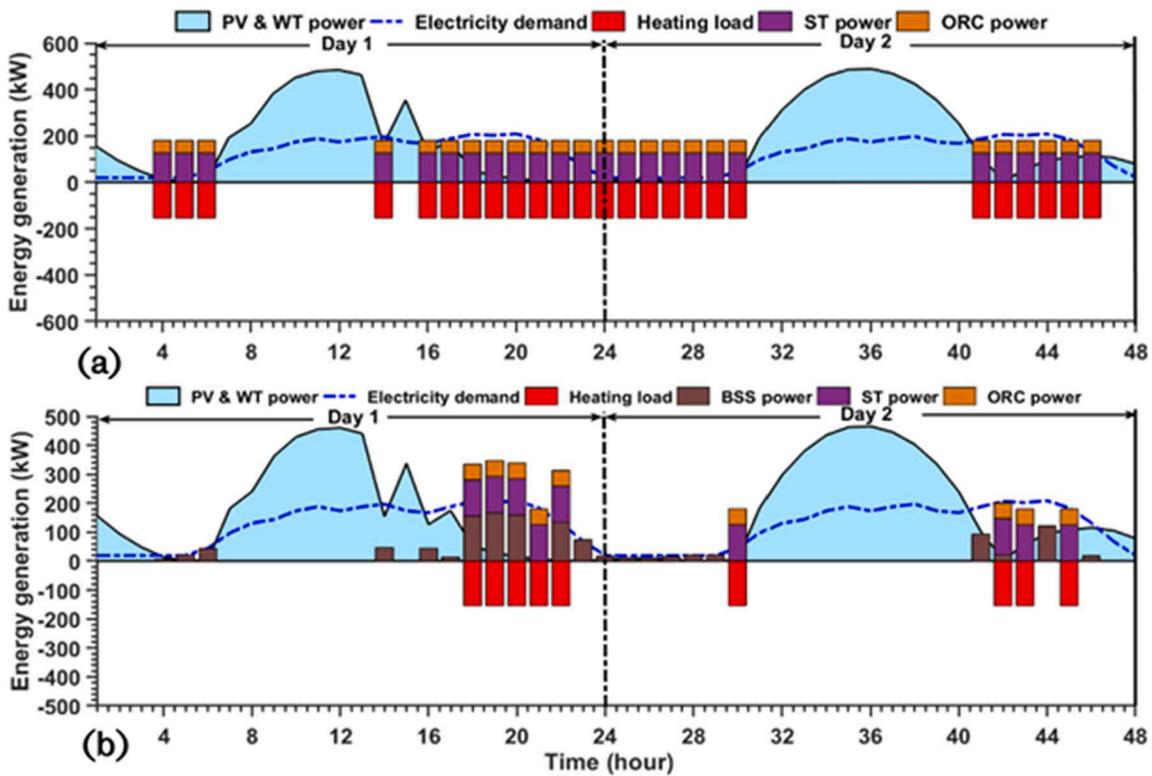
Fig. 14. Hourly generation of heating and commitment of the dispatchable generators in circuit charging (a) without battery and (b) with battery.

increase in the quality of the waste heat produced by the topping cycle in CC charging without battery (Fig. 12 or Fig. 14 (a)), the ORC is operated 25 times in the two days; the highest number of times for all the control strategies.

Overall, the deployment of battery storage minimises the commitment of the back-up to fulfilling the load and plays a crucial role in the reduction of the carbon emissions as well as the dumped power. Unfortunately, the inclusion of battery storage in the optimal system contributes to the increase in the frequency of start-ups of the ST back-up in the CC mode, because of the need to charge the batteries. Finally, BSS is more actively deployed in CC mode to fulfil the unmet load in the system in this test location compared to the LF mode.

6.2. Impact of dispatch strategies on the cooling generation

The investigation of the impact of the proposed control strategies on the cooling generation of the multi-carrier energy system is another notable contribution in this study. A single effect lithium bromide-water thermal chiller that has a fixed capacity of 96.6 kW has been deployed to produce the cooling and would be fired by the waste heat from the flue gas produced from woodchips combustion. Due to the unavailability of the cooling demand for the test location, this paper has been focused on the variation in the cooling generation from the proposed EMS.

Fig. 11 and Fig. 12 present the hourly generation of cooling effect by the thermal chiller when the biomass fired ST + ORC back-up is operational in the LF and CC control strategies, respectively. It is evident that the control strategies that deploy the programmable back-up more frequently produce more cooling (Fig. 11 (a) and Fig. 12 (a)). Hence, the LF and CC without battery produce more cooling (Fig. 11 (a) and Fig. 12 (a)) compared to the LF and CC with battery that deploy the ST + ORC

back-up few times to supply the deficit power as seen in Fig. 11 (b) and Fig. 12 (b), respectively. Finally, the absorption chiller is only deployed to produce cooling nine times (in two days) in control strategy 4 (Fig. 12 (b)), because batteries supply most of the unmet power in this strategy compared with any other control strategy and that shows the negative impact of deploying battery storage on cooling generation.

6.3. Impact of dispatch strategies on the heating generation

This section presents the simulated results of the impact of the proposed rule-based dispatch strategies on the heating generation of the multi-carrier system. Unlike in the case of the cooling generation, the capacity of the boiler in this case is determined by the available energy in the flue gas. In principle, the heating load and buffer storage will determine the amount of heating that is generated on an hourly basis [13]. Unfortunately, because the proposed system is designed for a remote test location, the daily hourly heating load is unknown. Hence, this simulation has been focused mainly on the generation potential of the energy vector.

Fig. 13 and Fig. 14 represent the hourly heating generation from the water boiler for the LF and CC control strategies proposed in this study, respectively. It is seen clearly in Fig. 13 and Fig. 14 that the heating generation varies for all the control strategies. In particular, as the commitment of the ST + ORC back-up in fulfilling the electric load increases, the generation of heating reduces, because less thermal energy is available to produce additional goods in the form of heating or hot water. The heating load generation is generally high in the LF mode (Fig. 13) compared with the CC (Fig. 14), because in the former, the ST + ORC back-up is

forced to follow the load. Hence, at most times in its operation, the ST main driver consumes a small fraction of the energy in the flue gas,
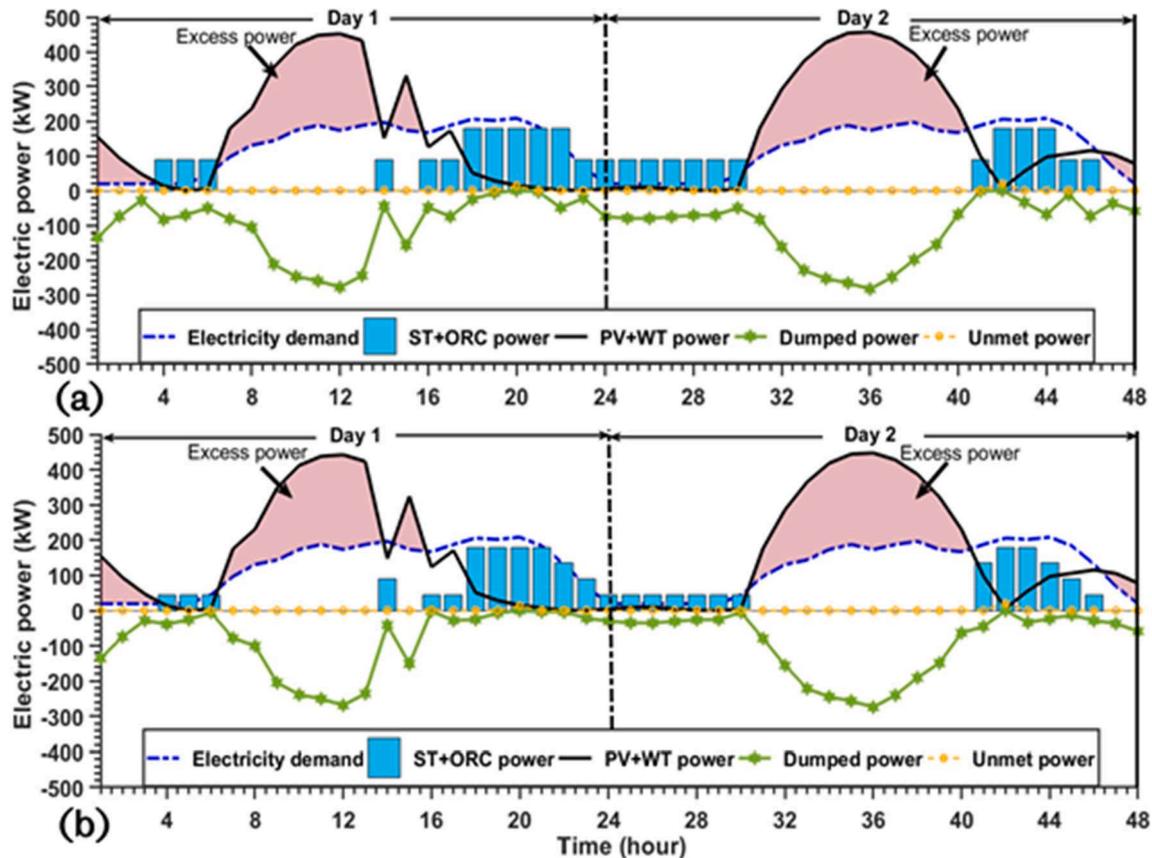
Fig. 15. Hourly commitments of the system units to meet the electricity load in circuit charging mode without battery storage for (a) 2-split ST and (b) 4-split ST cases.
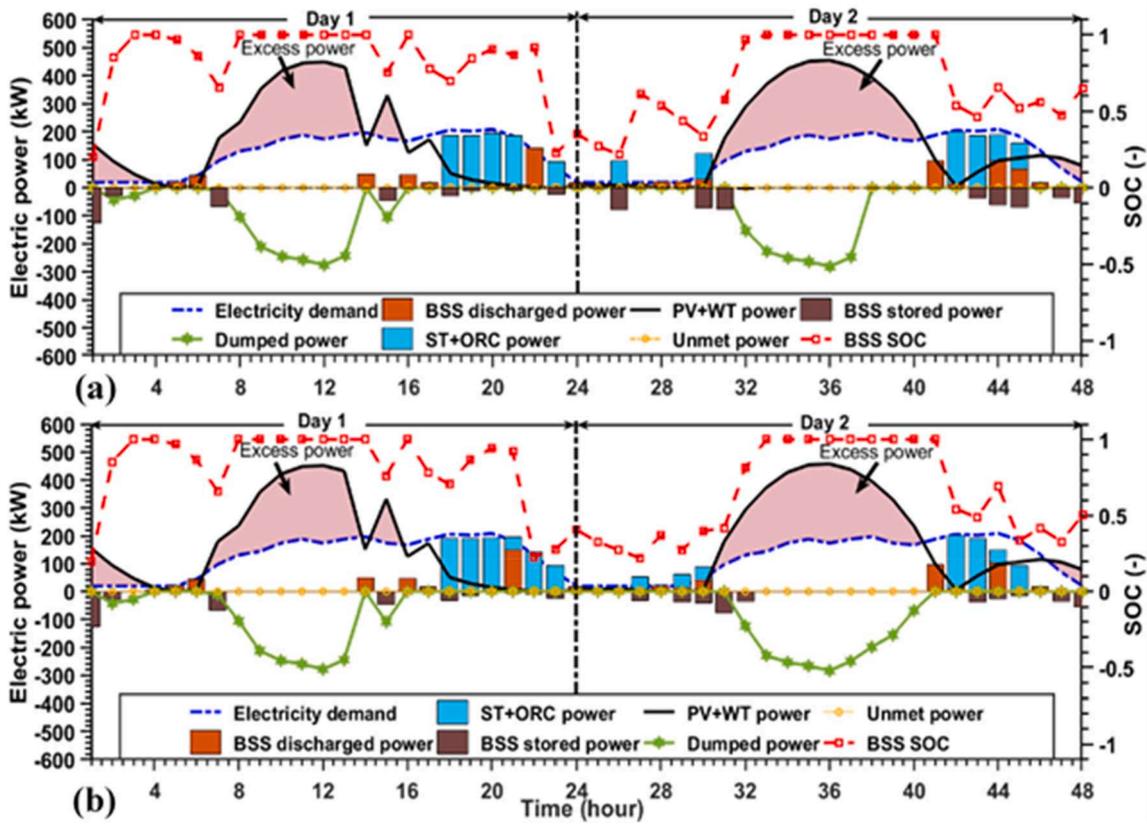
Fig. 16. Hourly commitments of the system units to meet the electricity load in circuit charging mode with battery storage for (a) 2-split ST and (b) 4-split ST cases.
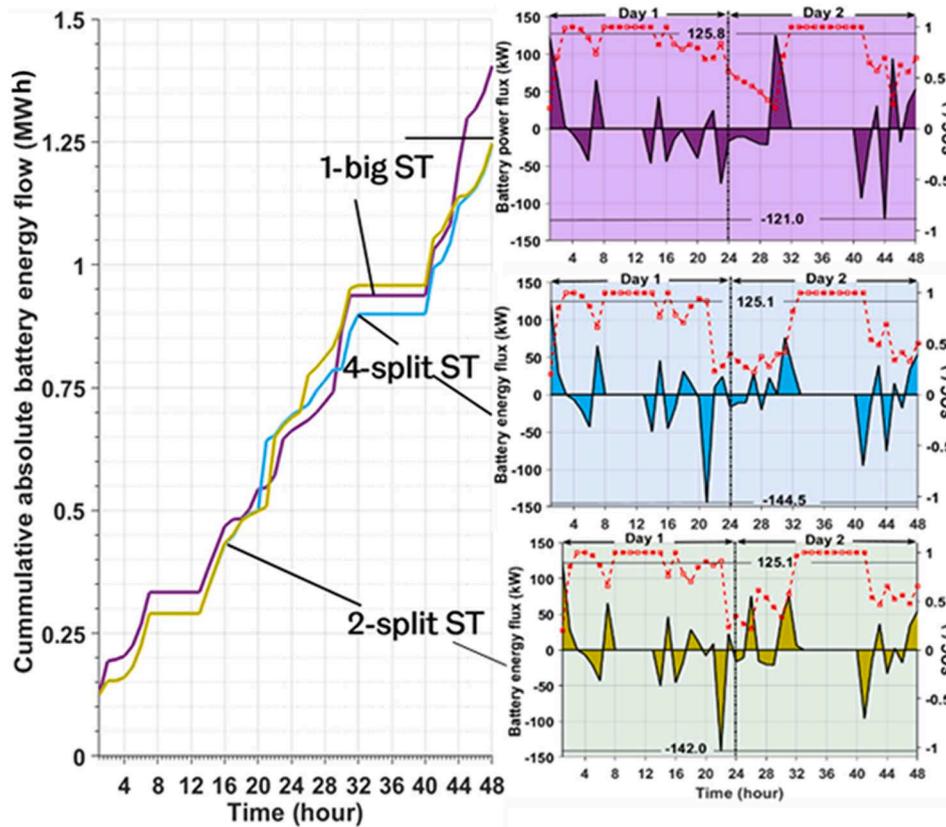
Fig. 17. Hourly energy flow through the batteries in circuit charging mode with split Stirling.

and this makes more energy available for the production of heating. In addition, since in the LF with battery storage (Fig. 13 (b)) the ST + ORC back-up does not produce excess power to charge the BSS, the system becomes more reliant on the dispatchable unit to fulfil the load in the absence of the green generators.

Overall, the CC with battery storage mode produces the least amount of heating, due to the increased deployment of batteries to supply the unmet power (Fig. 14 (b)). Finally, the inclusion of battery storage in the HRES design and the availability of the WT and PV generators affect the heating generation. Where batteries are not deployed to store the excess power produced by the renewable generators, more heating will be generated on days with poor weather, because of the inexorable increase in the dispatch of the ST + ORC back-up to fulfil the electricity demand. This is evident in the second day with fairly poor weather, in Fig. 13 and Fig. 14.

6.3.1. Impact of split of Stirling engine on electricity generation

The impact of deploying split ST to match the electric load of the test location has been evaluated for two split (2-split ST) and four split (4-split ST) ST cases. Split ST was only deployed in the CC strategy where it is applicable.

Fig. 15 and Fig. 16 represent the hourly commitments of the ST + ORC back-up and battery storage when split ST is deployed in CC to fulfill the electricity demand. It can be observed that the number of start-ups of the ST + ORC back-up is invariant when 2-split ST and 4-split ST were deployed to augment the positive net electric load without battery storage (Fig. 15 (a) and (b)). However, the dumped power from the system notably reduces, because of the reductions in the commitment of the back-up to fulfilling the load. The tangible reductions in the commitment of the back-up is responsible for the observed reductions in fuel consumption and emissions recorded in Table 8.

Conversely, in Fig. 16 (a) and (b) where 2-split and 4-split ST were deployed, respectively with battery storage, the number of start-ups of the back-up increases remarkably as the number of split increases. When compared with the case with one big ST (Fig. 9 (b)), it is seen that, with

the increase in the number of splits, the excess power produced by the dispatchable back-up reduces. Hence, it becomes difficult to charge the batteries once the non-programmable renewable generators are unavailable to generate excess power and this forces the ST + ORC back-up to operate more frequently.

Also, the introduction of the split ST concept impacts the battery negatively. Fig. 17 represents the cumulative energy flux through the batteries when 2-split and 4-split ST are deployed to match the unmet load in the system in CC mode. It is self-evident that the cumulative power handled by the BSS reduces with the increase in the number of small ST back-up. Further, the BSS noticeably undergoes deep discharge of power with the deployment of split back-up. When 4-split ST is deployed, the maximum discharged power is 144.5 kW compared to 121 kW recorded with 1-big ST. Meanwhile, the number of cycles of charging and discharging of the batteries increase with the deployment of split ST; however, comparable number of duty cycles are indicated for 2-split and 4-split cases. Apparently, the reduction in the ST back-up capacity with the increase in the number of splits suggests that the battery will be insufficiently charged; hence, the undesirable increase in the number of deep cycles that is inimical to the life of the battery [29].

On a positive note, the introduction of split ST minimises the dumping of excess power from the back-up, which also translates to the reduction in the fuel consumption. Additionally, with increasing number of split ST, the number of start-ups and operational hours of the ORC bottoming cycle reduce as it is evident in Figs. 18–21, because of the drop in the quality of the waste heat from the ST. For this reason, the operational cost of the system will reduce, i.e., the cost of maintenance and start-ups of the ORC and the reduction will be remarkable in the second day, where the ORC has been deployed for an average of 2.5 h in all the examined dispatch cases. Finally, it is evident that as the number of splits of the back-up increases, the behaviour of the energy system in CC mode tends towards that of LF mode. Consequently, the dumped power is minimised. Sadly, this is accompanied by some augmented costs, mainly driven by the additional commitments to the battery storage, but it offers some additional benefits by the efficient operation
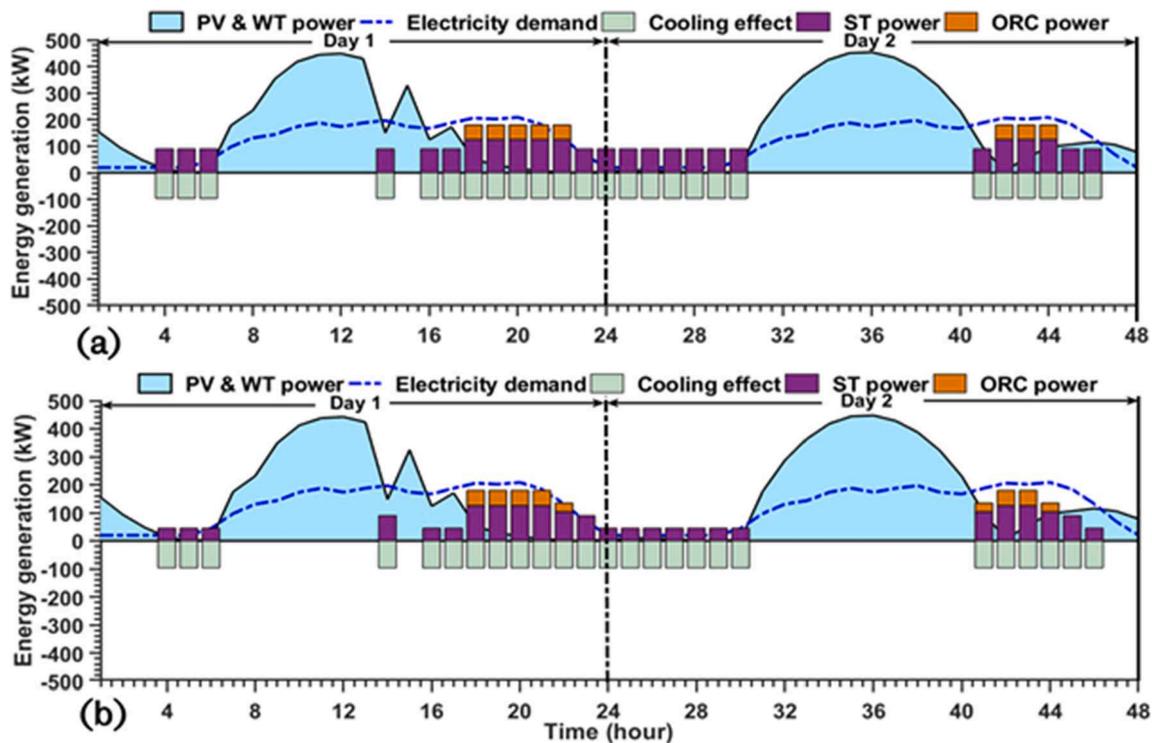
Fig. 18. Hourly generation of cooling and commitment of the dispatchable generators in circuit charging mode without battery storage for (a) 2-split ST and (b) 4-split ST cases.
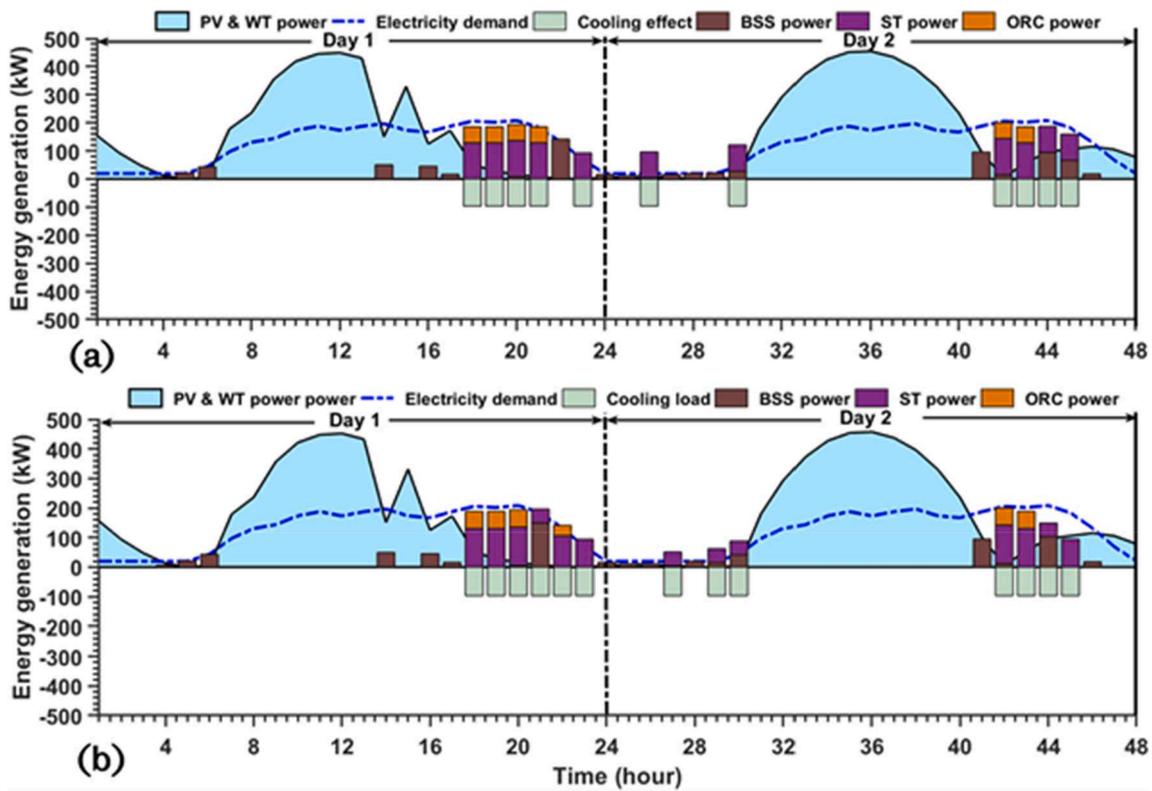
Fig. 19. Hourly generation of cooling and commitment of the dispatchable generators in circuit charging mode with battery storage for (a) 2-split ST and (b) 4-split ST cases.
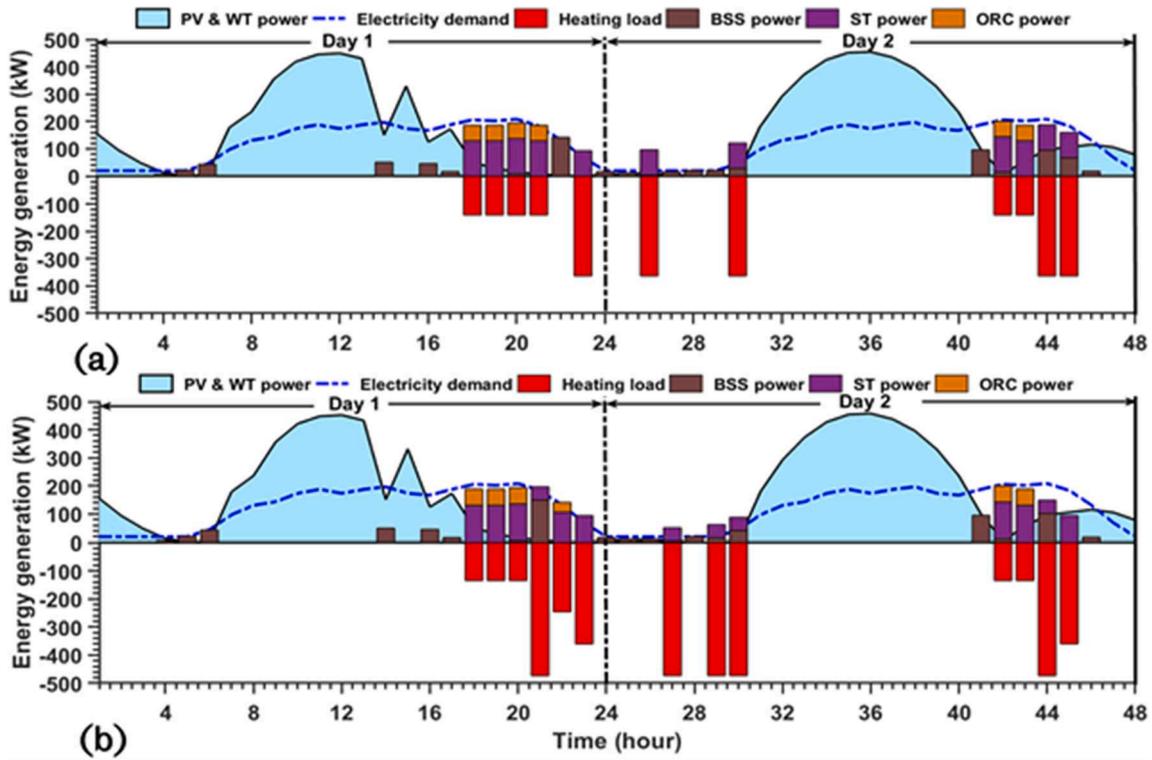
Fig. 20. Hourly generation of heating and commitment of the dispatchable generators in circuit charging mode without battery storage for (a) 2-split ST and (b) 4-split ST cases.
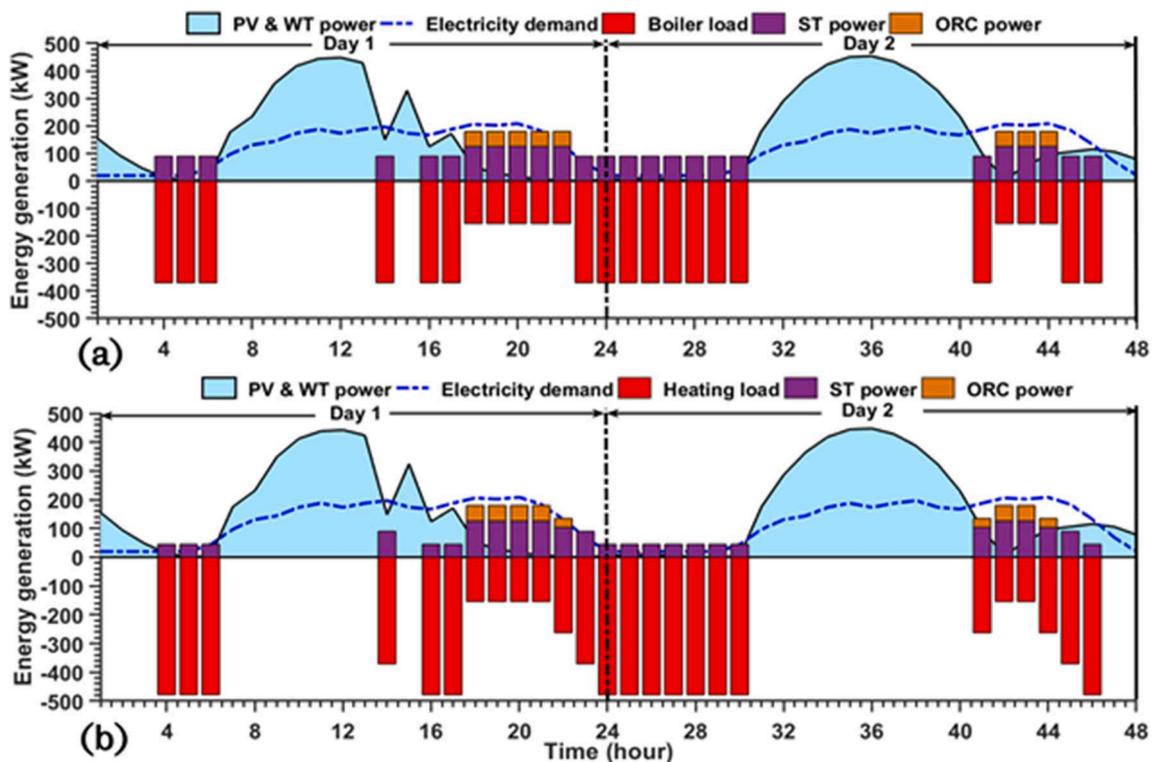
Fig. 21. Hourly generation of heating and commitment of the dispatchable generators in circuit charging mode with battery storage for (a) 2-split ST and (b) 4-split ST cases.

of the back-up, thereby minimising fuel consumption and carbon emissions.

6.3.2. Impact of split Stirling engine on cooling generation

Fig. 18 and Fig. 19 present the hourly generation of cooling by the thermal chiller when many small split ST are deployed in the CC mode to follow the electric load in the test location, without battery storage and with battery storage, respectively. It is seen from Fig. 18 (a) and (b) that the amount of cooling generation did not change with the deployment of two-split and four-split ST. This is because the operational hours and number of start-ups of the ST back-up were invariant with the increase in the number of splits. Consequently, the thermal chiller operates equal number of times regardless of the number of split back-up deployed. Also, if one notes that this generating unit can be operated satisfactorily with low grade heat of temperature less than 100 °C to provide cooling [46–48], the increase in the capacity of the ST which will reduce the quality of the flue gas, will not strongly affect its performance.

Contrarily, the generation of cooling increases with the increase in the number of splits as seen in Fig. 19 (a) and (b), due to the increase in the hours of operation of the ST back-up. Therefore, on cloudy days with less generation from the PV and WT, it is expected that there will be increase in the generation of cooling. Conclusively, while the inclusion of battery storage in the optimal system has a negative impact on the cooling generation, the combined deployment of battery storage and split ST favours the generation of cooling from the thermal chiller, because of the increased deployment of the back-up.

6.3.3. Impact of split Stirling engine on heating generation

The impact of deploying split Stirling engines on heating generation when the energy generation, storage and dispatch of the system is co-ordinated by the CC approach has been evaluated Fig. 20 and Fig. 21 illustrate the hourly generation of heating when 2-split ST and 4-split ST are deployed in CC without battery storage and with battery storage, respectively. It is evident in Fig. 20 (a) and (b) that the heating generation potential of the system more than doubled as the number of split of

the ST increases. As the number of split increases, the quality of the flue gas that is sent to the boiler increases, because of the reductions in the capacity of the ST. This reduction in the capacity of the ST suggests that less energy will be required to fire the heat engine.

Further, in Fig. 21 (a) and (b) where batteries were deployed, it has been remarked that the deployment of split ST in these cases, reduces the capacity of the back-up to charge the battery. Consequently, the number of times the ST is deployed increases; hence, the observed increase in the generation of heating with the increase in the number of splits. Day 2 that is marked with reduced period of generation from the renewables generates more heating than Day 1. Again, the combined inclusion of battery and split back-up in the optimal system configuration promotes the generation of heating.

7. Conclusion

In this paper, modified rule-based energy management strategies (EMS) have been proposed to coordinate the continuous generation, storage and dispatch of several energy vectors and other goods from a hybrid solar PV-wind and battery storage utilising the Stirling (ST) and ORC as back-up and prime mover of the integrated multi-carrier system. First, bi-level sizing optimisation has been deployed to obtain the optimal number of system components that minimises the system operational cost and offers cheap energy (LCOE), loss of power supply probability (LPSP), CO_2 emissions and dumped power in the outer-loop. While, the EMS was implemented in the inner-loop with the optimal system components including the control parameters generated in the outer-loop. Then, the best system configuration in each EMS case studied is selected from the Pareto optimal set by deploying the TOPSIS approach. Also, the hourly simulation of the optimal system configuration obtained in this study has been undertaken to highlight its dynamic behaviour in fulfilling the energy demand. It is evident that the choice of control strategy formulated to manage the multi-carrier system, plays a key role in determining the optimal system configuration. Based on the obtained results, the following conclusions are notable from this study:

- Inclusion of battery storage in the optimal system significantly improves the LPSP, LCOE, dumped power and CO_2 emissions of the HRES integrated multi-carrier system. However, while deploying battery storage reduces the number of start-ups of the back-up in the LF by 17%, it increases it by 51% in CC, increasing the operational cost. Consequently, the LCOE in LF is 4% less than in CC.
- Increment in the number of split ST remarkably reduces the LPSP, LCOE, CO_2 emissions and dumped power of the optimal system without battery storage and managed with the CC mode by 39.7%, 29.7%, 52.2% and 35.9%, respectively but has no influence on the number of start-ups of the back-up. Contrarily, increasing the number of split ST from 2 to 4 increases the operational cost of the system, because of the increase in the number of start-ups and results in a marginal increase in the LCOE.
- As the commitment of the ST to fulfilling the load reduces, the number of duty cycles of the battery storage increases because of the reduction in the capacity of the back-up to charge the batteries, and this would contribute to high wear of the batteries. Also, an increase in the number of small ST reduces the quality of the waste heat produced from the ST topping cycle, thereby minimising the number of times the auxiliary ORC back-up is deployed.
- While the generation of heating and cooling reduces with the inclusion of battery storage in the optimal system. It, however, increases with the combined deployment of battery storage and split ST, because of the increase in the quality of the combustion flue that powers the boiler.

Finally, the proposed modified traditional rule-based energy management system, which deploys split ST back-up, reduces the dumping of power and emissions from the optimal system, by reducing the hourly commitments of the back-up in fulfilling the load. In addition, it enhances the cooling and heating generation potentials of the multi-carrier energy system, by improving the quality of the combustion flue sent to these units. Although it produces many cycles of charging and discharging of the battery storage when compared to the traditional LF and CC and augments the operational cost by increasing the number of start-ups of the split back-up, the LCOE is still slightly lower because of the tremendous reductions in the commitment of the back-up. However, the LCOE can be enhanced by simultaneously prioritising the charging of the batteries and fulfilment of the load in the dispatch of the split-back up and will be studied in a future work.

CRediT authorship contribution statement

Godfrey T. Udeh: Conceptualization, Methodology, Software, Data curation, Validation, Investigation, Formal analysis, Writing – original draft, Writing – review & editing, Funding acquisition. **Stavros Michailos:** Conceptualization, Formal analysis, Validation, Data curation, Writing – review & editing. **Derek Ingham:** Project administration, Visualization, Writing – review & editing. **Kevin J. Hughes:** Project administration, Writing – review & editing, Supervision. **Lin Ma:** Conceptualization, Writing – review & editing, Visualization, Supervision. **Mohamed Pourkashanian:** Project administration, Supervision.

Declaration of Competing Interest

The authors declare that they have no known competing financial interests or personal relationships that could have appeared to influence the work reported in this paper.

Acknowledgements

Appendix A. Supplementary material

Supplementary data to this article can be found online at https://doi.org/10.1016/j.apenergy.2022.118763.

References

[1] Olatomiwa L, Mekhilef S, Ismail MS, Moghavvemi M. Energy management strategies in hybrid renewable energy systems: A review. Renew Sustain Energy Rev 2016;62:821–35. https://doi.org/10.1016/j.rser.2016.05.040.

[2] Ammari C, Belatrache D, Touhami B, Makhloufi S. Sizing, optimization, control and energy management of hybrid renewable energy system- a review. Energy Built Environ 2021. https://doi.org/10.1016/j.enbenv.2021.04.002.

[3] Olatomiwa L, Mekhilef S, Ohunakin OS. Hybrid renewable power supply for rural health clinics (RHC) in six geo-political zones of Nigeria. Sustain Energy Technol Assessments 2016;13:1–12. https://doi.org/10.1016/j.seta.2015.11.001.

[4] Sawle Y, Gupta SC, Bohre AK. Optimal sizing of standalone PV/Wind/Biomass hybrid energy system using GA and PSO optimization technique. Energy Procedia 2017;117:690–8. https://doi.org/10.1016/j.egypro.2017.05.183.

[5] Azaza M, Wallin F. Multi objective particle swarm optimization of hybrid micro-grid system: A case study in Sweden. Energy 2017;123:108–18. https://doi.org/10.1016/j.energy.2017.01.149.

[6] Baghaee HR, Mirsalim M, Gharehpetian GB. Multi-objective optimal power management and sizing of a reliable wind/PV microgrid with hydrogen energy storage using MOPSO. J Intell Fuzzy Syst 2017;32(3):1753–73. https://doi.org/10.3233/JIFS-152372.

[7] Dufo-López R, Lujano-Rojas JM, Bernal-Agustín JL. Comparison of different lead-acid battery lifetime prediction models for use in simulation of stand-alone photovoltaic systems. Appl Energy 2014;115:242–53. https://doi.org/10.1016/j.apenergy.2013.11.021.

[8] Al-Masri HMK, Al-Sharqi AA. Technical design and optimal energy management of a hybrid photovoltaic biogas energy system using multi-objective grey Wolf optimisation. IET Renew Power Gener 2020;14(14):2765–78. https://doi.org/10.1049/iet-rpg.2020.0330.

[9] Gupta A, Saini RP, Sharma MP. Modelling of hybrid energy system-Part II: Combined dispatch strategies and solution algorithm. Renew Energy 2011;36(2):466–73. https://doi.org/10.1016/j.renene.2009.04.035.

[10] Das BK, Zaman F. Performance analysis of a PV/Diesel hybrid system for a remote area in Bangladesh: Effects of dispatch strategies, batteries, and generator selection. Energy 2019;169:263–76. https://doi.org/10.1016/j.energy.2018.12.014.

[11] Ogunjuyigbe ASO, Ayodele TR, Akinola OA. Optimal allocation and sizing of PV/Wind/Split-diesel/Battery hybrid energy system for minimizing life cycle cost, carbon emission and dump energy of remote residential building. Appl Energy 2016;171:153–71. https://doi.org/10.1016/j.apenergy.2016.03.051.

[12] Das BK, Al-Abdeli YM, Kothapalli G. Optimisation of stand-alone hybrid energy systems supplemented by combustion-based prime movers. Appl Energy 2017;196:18–33. https://doi.org/10.1016/j.apenergy.2017.03.119.

[13] Mazzola S, Astolfi M, Macchi E. A detailed model for the optimal management of a multigood microgrid. Appl Energy 2015;154:862–73. https://doi.org/10.1016/j.apenergy.2015.05.078.

[14] Silvente J, Papageorgiou LG. An MILP formulation for the optimal management of microgrids with task interruptions. Appl Energy 2017;206:1131–46. https://doi.org/10.1016/j.apenergy.2017.08.147.

[15] Parisio A, Rikos E, Glielmo L, Member S. A model predictive control approach to microgrid operation optimization 2014;22:1813–27.

[16] Forough AB, Roshandel R. Lifetime optimization framework for a hybrid renewable energy system based on receding horizon optimization. Energy 2018;150:617–30. https://doi.org/10.1016/j.energy.2018.02.158.

[17] Li B, Roche R, Miraoui A. Microgrid sizing with combined evolutionary algorithm and MILP unit commitment. Appl Energy 2017;188:547–62. https://doi.org/10.1016/j.apenergy.2016.12.038.

[18] Rullo P, Braccia L, Luppi P, Zumoffen D, Feroldi D. Integration of sizing and energy management based on economic predictive control for standalone hybrid renewable energy systems. Renew Energy 2019;140:436–51. https://doi.org/10.1016/j.renene.2019.03.074.

[19] Dufo-López R, Bernal-Agustín JL, Yusta-Loyo JM, Domínguez-Navarro JA, Ramírez-Rosado IJ, Lujano J, et al. Multi-objective optimization minimizing cost and life cycle emissions of stand-alone PV-wind-diesel systems with batteries storage. Appl Energy 2011;88(11):4033–41. https://doi.org/10.1016/j.apenergy.2011.04.019.

[20] Bukar AL, Tan CW, Yiew LK, Ayop R, Tan W-S. A rule-based energy management scheme for long-term optimal capacity planning of grid-independent microgrid optimized by multi-objective grasshopper optimization algorithm. Energy Convers Manage 2020;221:113161. https://doi.org/10.1016/j.enconman.2020.113161.

[21] Sun B. A multi-objective optimization model for fast electric vehicle charging stations with wind, PV power and energy storage. J Clean Prod 2021;288:125564. https://doi.org/10.1016/j.jclepro.2020.125564.

[22] Lu X, Zhou K, Yang S. Multi-objective optimal dispatch of microgrid containing electric vehicles. J Clean Prod 2017;165:1572–81. https://doi.org/10.1016/j.jclepro.2017.07.221.

[23] Bracco S, Delfino F, Pampararo F, Robba M, Rossi M. A mathematical model for the optimal operation of the University of Genoa Smart Polygeneration Microgrid:

Evaluation of technical, economic and environmental performance indicators. Energy 2014;64:912–22. https://doi.org/10.1016/j.energy.2013.10.039.

[24] Bhatti AR, Salam Z. A rule-based energy management scheme for uninterrupted electric vehicles charging at constant price using photovoltaic-grid system. Renew Energy 2018;125:384–400. https://doi.org/10.1016/j.renene.2018.02.126.

[25] Cristóbal-Monreal IR, Dufo-López R. Optimisation of photovoltaic-diesel-battery stand-alone systems minimising system weight. Energy Convers Manag 2016;119: 279–88. https://doi.org/10.1016/j.enconman.2016.04.050.

[26] Models WT. Wind Turbines n.d. www.en.wind-turbine-models.com (accessed June 1, 2021).

[27] Bhandari B, Poudel SR, Lee K-T, Ahn S-H. Mathematical modeling of hybrid renewable energy system: A review on small hydro-solar-wind power generation. Int J Precis Eng Manuf Technol 2014;1(2):157–73. https://doi.org/10.1007/s40684-014-0021-4.

[28] Lujano-Rojas JM, Dufo-López R, Bernal-Agustín JL. Optimal sizing of small wind/battery systems considering the DC bus voltage stability effect on energy capture, wind speed variability, and load uncertainty. Appl Energy 2012;93:404–12. https://doi.org/10.1016/j.apenergy.2011.12.035.

[29] Dufo-López R, Cristóbal-Monreal IR, Yusta JM. Optimisation of PV-wind-diesel-battery stand-alone systems to minimise cost and maximise human development index and job creation. Renew Energy 2016;94:280–93. https://doi.org/10.1016/j.renene.2016.03.065.

[30] PV GIS. Satellite data n.d. https://ec.europa.eu/jrc/en/PVGIS/releases/pvgis51 (accessed January 8, 2021).

[31] Udeh GT, Michailos S, Ingham D, Hughes KJ, Ma L, Pourkashanian M. A techno-enviro-economic assessment of a biomass fuelled micro-CCHP driven by a hybrid Stirling and ORC engine. Energy Convers Manag 2021;227:113601. https://doi.org/10.1016/j.enconman.2020.113601.

[32] Badea N. Design for Micro-Combined Cooling, Heating and Power Systems. Springer Berlin Heidelberg; 2015. https://doi.org/10.1007/978-1-4471-6254-4.

[33] Cozzolino R, Tribioli L, Bella G. Power management of a hybrid renewable system for artificial islands: A case study. Energy 2016;106:774–89. https://doi.org/10.1016/j.energy.2015.12.118.

[34] ICPC. ICPC report on emissions n.d. http://www.ipcc-nggip.iges.or.jp/public/2006gl/pdf/2_Volume2/V2_2_Ch2_Stationary_Combustion.pdf.

[35] HOPPECKE Sun Power n.d. https://voltaconsolar.com/batteries/agm-lead-acid/hoppecke-sun-power.html (accessed February 5, 2021).

[36] Solaris. Candian Solar Panel n.d. https://www.solaris-shop.com/canadian-solar-kumax-cs3u-340p-340w-poly-solar-panel/ (accessed March 6, 2021).

[37] Lu J, Wang W, Zhang Y, Cheng S. Multi-Objective Optimal Design of Stand-Alone Hybrid Energy System Using Entropy Weight Method Based on HOMER. Energies 2017;10:1664. https://doi.org/10.3390/en10101664.

[38] Moradi H, Esfahanian M, Abtahi A, Zilouchian A. Optimization and energy management of a standalone hybrid microgrid in the presence of battery storage system. Energy 2018;147:226–38. https://doi.org/10.1016/j.energy.2018.01.016.

[39] Ramli MAM, Bouchekara HREH, Alghamdi AS. Optimal sizing of PV/wind/diesel hybrid microgrid system using multi-objective self-adaptive differential evolution algorithm. Renew Energy 2018;121:400–11. https://doi.org/10.1016/j.renene.2018.01.058.

[40] National Renewable Energy Laboratory. U.S. Solar Photovoltaic System and Energy Storage Cost Benchmark: Q1 2020. 2021.

[41] Entezari A, Manizadeh A, Ahmadi R. Energetical, exergetical and economical optimization analysis of combined power generation system of gas turbine and Stirling engine. Energy Convers Manag 2018;159:189–203. https://doi.org/10.1016/j.enconman.2018.01.012.

[42] Quoilin S, Van Den BM, Declaye S, Dewallef P, Lemort V. Techno-economic survey of organic rankine cycle (ORC) systems. Renew Sustain Energy Rev 2013;22: 168–86. https://doi.org/10.1016/j.rser.2013.01.028.

[43] Tégani I, Aboubou A, Ayad MY, Becherif M, Saadi R, Kraa O. Optimal sizing design and energy management of stand-alone photovoltaic/wind generator systems. Energy Procedia 2014;50:163–70. https://doi.org/10.1016/j.egypro.2014.06.020.

[44] Nigerian Rural Electrification Agency. Nigeria minigrid investment brief 2017:25.

[45] Lujano-Rojas JM, Dufo-López R, Atencio-Guerra JL, Rodrigues EMG, Bernal-Agustín JL, Catalão JPS. Operating conditions of lead-acid batteries in the optimization of hybrid energy systems and microgrids. Appl Energy 2016;179: 590–600. https://doi.org/10.1016/j.apenergy.2016.07.018.

[46] Somers C, Mortazavi A, Hwang Y, Radermacher R, Rodgers P, Al-Hashimi S. Modeling water/lithium bromide absorption chillers in ASPEN Plus. Appl Energy 2011;88(11):4197–205. https://doi.org/10.1016/j.apenergy.2011.05.018.

[47] Wang K, Abdelaziz O, Kisari P, Vineyard EA. State-of-the-art review on crystallization control technologies for water/LiBr absorption heat pumps. Int J Refrig 2011;34(6):1325–37. https://doi.org/10.1016/j.ijrefrig.2011.04.006.

[48] Srikhirin P, Aphornratana S, Chungpaibulpatana S. A review of absorption refrigeration technologies. Renew Energy Rev 2001;5:343–72. https://doi.org/10.1136/bmj.290.6471.860-a.